

Quantum-Enhanced Transmittance Sensing

Zihao Gong, *Student Member, IEEE*, Nathaniel Rodriguez, *Student Member, IEEE*, Christos N. Gagatsos, Saikat Guha, *Senior Member, IEEE*, and Boulat A. Bash, *Member, IEEE*

Abstract—We consider the problem of estimating unknown transmittance η of a target bathed in thermal background light. As quantum estimation theory yields the fundamental limits, we employ lossy thermal noise bosonic channel model, which describes sensor-target interaction quantum-mechanically in many practical active-illumination systems (e.g., using emissions at optical, microwave, or radio frequencies). We prove that quantum illumination using two-mode squeezed vacuum (TMSV) states asymptotically achieves minimal quantum Cramér-Rao bound (CRB) over all quantum states (not necessarily Gaussian) in the limit of small input photon number. We characterize the optimal receiver structure for TMSV input and show its advantage over other receivers using both analysis and Monte Carlo simulation.

I. INTRODUCTION AND PROBLEM SETUP

A precise measurement of power transmittance is a fundamental task in engineering. In active sensing, power transmittance translates to target reflectance, making its estimation central to RADAR and LIDAR. Signal attenuation is a major source of distortion in communications, making transmittance measurement critical in channel state estimation. Furthermore, transmittance plays a crucial role in quantum system design. It determines the ultimate limit of any point-to-point quantum communication protocol [2], whether the lossy thermal noise bosonic channel is entanglement-breaking [3], and how close quantum metrology methods are to the Heisenberg limit for phase estimation [4], [5].

Classical linear channel relates the complex-valued input and output amplitude mode functions a and b by $b = \sqrt{\eta}a + z$, where η is power transmittance and z is additive noise. Using an independent Gaussian random variable to represent noise z yields an additive white Gaussian noise (AWGN) channel, and simplifies estimation of transmittance η [6].

Consider measurement of transmittance in an optical channel. Light is an electromagnetic wave described quantum-mechanically by a boson field. Noises of quantum-mechanical origin limit the performance of advanced high-sensitivity photodetection systems [7]–[9]. Therefore, achieving the ultimate

Section II and parts of Section I and IV of this article were presented at the International Symposium on Information Theory (ISIT 2021) [1].

ZG and BAB were supported by the National Science Foundation (NSF) under Grant No. CCF-2045530. NR was supported by the NSF under Grant Nos. EEC-1941583 and CCF-2006679. CNG and SG acknowledge funding support from the Office of Naval Research, grant number N00014-19-1-2189.

Zihao Gong and Nathaniel Rodriguez are with Electrical and Computer Engineering Department, The University of Arizona, Tucson, AZ 85721 USA (email: zihao@arizona.edu and nrod968@email.arizona.edu).

Christos N. Gagatsos is with the College of Optical Sciences, The University of Arizona, Tucson, AZ 85721 USA (email: cgagatsos@email.arizona.edu).

Saikat Guha and Boulat A. Bash are with the Electrical and Computer Engineering Department, The University of Arizona, Tucson, AZ 85721 USA, and also with the College of Optical Sciences, The University of Arizona, Tucson, AZ 85721 USA (email: saikat@optics.arizona.edu and boulat@arizona.edu).

limits of estimation generally requires tools from quantum information processing [10], [11] and quantum optics [12]–[14]. A single-mode lossy thermal noise bosonic channel $\mathcal{E}_{S \rightarrow R}^{\bar{n}_T, \eta}$ in Fig. 1 describes quantum-mechanically the transmission of a single (spatio-temporal-polarization) mode of the electromagnetic field at a given transmission wavelength (such as optical or microwave) over linear loss and additive Gaussian noise (such as noise stemming from blackbody radiation). A beamsplitter with transmissivity η models loss. In contrast to the classical linear model, here the input-output relationship $\hat{b} = \sqrt{\eta}\hat{a} + \sqrt{1-\eta}\hat{e}$ between the bosonic modal annihilation operators of the single-mode channel requires the environment mode \hat{e} to preserve the unitarity by ensuring that commutator $[\hat{b}, \hat{b}^\dagger] = 1$. Noise is modeled by mode \hat{e} being in a zero-mean thermal state $\hat{\tau}_{\bar{n}_T}$, where \bar{n}_T is the mean photon number per mode injected by the environment.

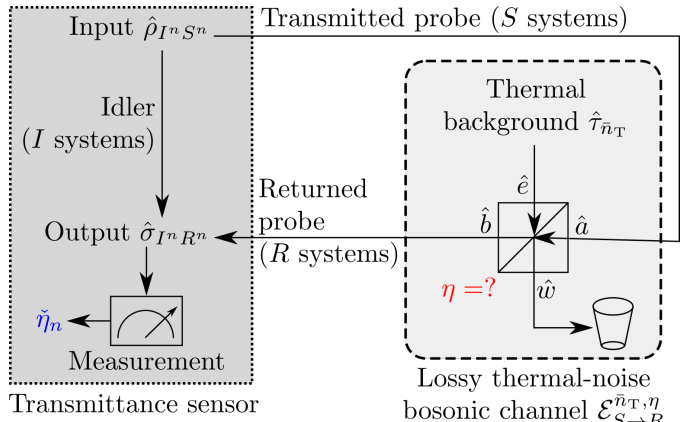


Fig. 1. Sensing of unknown transmittance η . Sensor transmits n -mode signal systems S of bipartite state $\hat{\rho}_{I^n S^n}$ by using n times the single-mode thermal noise lossy bosonic channel $\mathcal{E}_{S \rightarrow R}^{\eta, \bar{n}_T}$ modeled by a beamsplitter with transmissivity η and an environment injecting a thermal state $\hat{\tau}_{\bar{n}_T}$ with mean photon number $\bar{n}_T \equiv \frac{\bar{n}_B}{1-\eta}$. \hat{a} , \hat{b} , \hat{e} , and \hat{w} label input/output modal annihilation operators for the bosonic channel. Idler systems I are retained as a reference for the measurement of output state $\hat{\sigma}_{I^n R^n}$, which yields the estimator $\check{\eta}_n$.

Although the channel $\mathcal{E}_{S \rightarrow R}^{\bar{n}_T, \eta}$ is fixed, quantum mechanics allows the choice of modulation state for input mode \hat{a} and measurement for output mode \hat{b} . A classical channel is created by fixing these choices, which may be suboptimal. For example, AWGN channel arises when laser light modulation is used at the transmitter (i.e., \hat{a} is excited in a coherent state) and coherent detection (homodyne or heterodyne) is used at the receiver. However, these choices double the mean squared error (MSE) of transmittance estimation (see Section IV). Quantum information processing seeks to optimize input states and measurements on the output states. This approach led to significant advances in sensing [15], [16]. However,

despite progress in quantum transmittance estimation without noise ($\bar{n}_T = 0$) [17], [18], the complete methodology that accounts for thermal noise ($\bar{n}_T > 0$) and includes receiver design has been elusive.

Fig. 1 depicts the quantum-information model of transmittance sensing. The sensor prepares a bipartite quantum input state $\hat{\rho}_{I^n S^n}$ which occupies n signal systems S and n idler systems I . Signal systems S interrogate the target over n available modes of channel $\mathcal{E}_{S \rightarrow R}^{\bar{n}_T, \eta}$. Idler systems I are retained as lossless and noiseless reference. The output state $\hat{\sigma}_{I^n R^n} = (\mathcal{I}_I \otimes \mathcal{E}_{S \rightarrow R}^{\bar{n}_T, \eta})^{\otimes n} [\hat{\rho}_{I^n S^n}]$ carries information about transmittance η in the returned systems R . The estimator $\hat{\eta}_n$ measures $\hat{\sigma}_{I^n R^n}$, and minimizes the mean squared error $\text{MSE}_\eta \equiv E[(\hat{\eta}_n - \eta)^2]$, where $E[\cdot]$ denotes expectation. For an unbiased $\hat{\eta}_n$, the quantum Cramér-Rao bound (CRB) is $\text{MSE}_\eta \geq \frac{1}{\mathcal{J}_\eta(\hat{\sigma}_{I^n R^n})}$, where $\mathcal{J}_\eta(\hat{\sigma}_{I^n R^n})$ is the quantum Fisher information (QFI) associated with η for state $\hat{\sigma}_{I^n R^n}$.

Quantum illumination (QI) approaches improve detection and estimation in noise using entanglement between S and I . The quantum CRB for joint estimation of unknown η and \bar{n}_T using Gaussian states [19] was derived in [20], with the two-mode squeezed vacuum (TMSV) states proved optimal. However, in [20] the sensor can estimate η from just the thermal background, while much of the QI literature [21]–[26] assumes that the thermal background cannot aid in the estimation of the parameter of interest. This is typically done by setting $\bar{n}_T \equiv \frac{\bar{n}_B}{1-\eta}$, where \bar{n}_B is the mean number of thermal background photons/mode that corrupt sensor's probes. When the background light does not help the estimation of η , quantum CRB is quantitatively different from results in [20]¹, and the QFI is upper-bounded by [21, Eq. (21)]:

$$\mathcal{J}_\eta(\hat{\sigma}_{I^n R^n}) \leq \mathcal{J}_{\eta, \text{ub}}(\bar{N}_S) \equiv \frac{\bar{N}_S}{\eta(\bar{n}_B + 1 - \eta)}, \quad (1)$$

where \bar{N}_S is the total mean photon number transmitted over n modes. However, [21] leaves open the structure of $\hat{\rho}_{I^n S^n}$ that saturates (1), and the design of the measurement that achieves the corresponding quantum CRB. Recent work [27] investigates transmittance sensing using Gaussian states [19] and with and without noise aiding the estimation. While their treatment of QFI is comprehensive, they do not consider receiver structures that achieve QFI.

Summary of our results and their significance: The authors of [21] question whether a regime exists where (1) is saturated for arbitrary η and $\bar{n}_B > 0$. We answer affirmatively in the next section by proving that a product of n TMSV states achieves the bound in (1) in the limit of small mean photon number per mode $\bar{n}_S \equiv \frac{\bar{N}_S}{n}$. This adds to the many positive features of TMSV states and suggests QI protocol for transmittance sensing. Low input power regime has significant practical applications to sensors operating under total power constraints, e.g., imposed by covertness/low probability of detection (LPD) [28]–[35] or battery size.

Therefore, in Section III, we derive a receiver structure that achieves quantum CRB asymptotically as $n \rightarrow \infty$ when

¹Reparametrizing [20, Eqs. (B8a)–(B8d)] to $\eta = e^{-\gamma}$ shows that, even in the absence of probes ($\bar{n}_S = 0$), QFI associated with η is positive due to the thermal background.

TMSV is input and maximum likelihood estimation (MLE) is performed on the classical output of the receiver. Therefore, it is optimal in the low input power regime. Our receiver is constructed from well-known optical components: a two-mode squeezer followed by photon number resolving (PNR) measurement. However, despite this convenience, our receiver's existence is limited to a certain range of η , \bar{n}_S , and \bar{n}_B . Thus, in Section IV, we compare its theoretical limits to those of other well-known receivers, and show significant advantage derived from using TMSV input and our receiver.

The MSE of the system using TMSV input, our receiver, and MLE on its output converges to quantum CRB as $n \rightarrow \infty$. However, practical sensing is limited to finite number of observations: $n < \infty$. This motivates evaluating the speed of convergence to CRB. Further complicating the analysis is the fact that the structure of our receiver depends on the parameter of interest η . This is common in quantum estimation, and is addressed using the two-stage method from [36], [37], [38, Ch. 6.4], which achieves quantum CRB as $n \rightarrow \infty$. In Section V we use a Monte Carlo simulation to study the performance of transmittance sensing at $n < \infty$ that uses TMSV input with our receiver and an OPA receiver, as well as a coherent transceiver. We show that the MSEs for these systems converge rapidly to corresponding quantum CRBs even when two-stage method is used.

Unlike previous QI schemes which demonstrated advantage in the highly unusual regime of high noise and low signal-to-noise ratio (SNR) [21]–[26], our protocol shows substantial improvement over classical approach in the low noise regime. In fact, our method shows particular promise for transmittance measurement in the near-field optical channels. Such channels have low but positive \bar{n}_B , η significantly above zero, and have applications in quantum reading [39] and metropolitan free-space optical networks [40]. We argue that, although technically challenging, an experimental validation of our design is feasible in the near term, as the required squeezing and photon number resolution have been demonstrated. We conclude with a discussion of future work in Section VI.

II. TMSV IS OPTIMAL FOR TRANSMITTANCE SENSING

The TMSV state is represented in the Fock (photon number) basis as follows:

$$|\psi\rangle_{IS} = \sum_{k=0}^{\infty} \sqrt{q(k; \bar{n}_S)} |k\rangle_I |k\rangle_S, \quad (2)$$

where the Bose-Einstein probability mass function

$$q(k; \bar{n}) = \frac{\bar{n}^k}{(1 + \bar{n})^{k+1}} \quad (3)$$

is a variant of a geometric distribution. TMSV is a zero-displacement pure Gaussian state, which among all two-mode Gaussian states with mean photon number \bar{n}_S is maximally-entangled [19]. It is critical in quantum information processing and can be readily generated. We show that TMSV becomes optimal for transmittance estimation in thermal noise as input photon number per mode decays to zero:

Theorem 1. *The following limit holds for the quantum Fisher information $\mathcal{J}_\eta(\hat{\sigma}_{I^n R^n})$:*

$$\lim_{\bar{n}_S \rightarrow 0} \frac{\mathcal{J}_\eta(\hat{\sigma}_{I^n R^n})}{\bar{n}_S} = \frac{n}{\eta(\bar{n}_B + 1 - \eta)} \quad (4)$$

when product TMSV input state $\hat{\rho}_{I^n S^n} = |\psi\rangle\langle\psi|_{IS}^{\otimes n}$ is used.

Proof: Since the bosonic channel acts independently on each transmitted mode, for input state $|\psi\rangle\langle\psi|_{IS}^{\otimes n}$, the output state $\hat{\sigma}_{I^n R^n} = \hat{\sigma}_{IR}^{\otimes n}(\eta)$ is a product of states $\hat{\sigma}_{IR}(\eta) = (\mathcal{I}_I \otimes \mathcal{E}_{S \rightarrow R}^{\bar{n}_T, \eta})[|\psi\rangle\langle\psi|_{IS}]$ which we parametrize by η . Thus, by the additivity of the QFI for product states, $\mathcal{J}_\eta(\hat{\sigma}_{I^n R^n}) = n\mathcal{J}_\eta(\hat{\sigma}_{IR}(\eta))$. Furthermore, the bosonic channel is Gaussian, allowing the use of the symplectic formalism [19]. We employ the $\hat{q}\hat{q}\hat{p}\hat{p}$ form for representing and evolving the covariance matrices of Gaussian states in phase-space, where $\hat{q} = \frac{\hat{a} + \hat{a}^\dagger}{\sqrt{2}}$ and $\hat{p} = \frac{\hat{a} - \hat{a}^\dagger}{i\sqrt{2}}$ are the quadrature operators. The input TMSV state's covariance matrix is:

$$\Sigma_{\hat{\rho}_{IS}} = \begin{bmatrix} u_1 & u_2 & 0 & 0 \\ u_2 & u_1 & 0 & 0 \\ 0 & 0 & u_1 & -u_2 \\ 0 & 0 & -u_2 & u_1 \end{bmatrix}, \quad (5)$$

where $u_1 = \bar{n}_S + \frac{1}{2}$ and $u_2 = \sqrt{\bar{n}_S(\bar{n}_S + 1)}$. The action of the lossy thermal noise bosonic channel on the signal mode does not displace the state and results in the covariance matrix of the output:

$$\Sigma_{\hat{\sigma}_{IR}(\eta)} = X \Sigma_{\hat{\rho}_{IS}} X^T + Y \quad (6)$$

$$= \begin{bmatrix} w_{11} & w_{12} & 0 & 0 \\ w_{12} & w_{22} & 0 & 0 \\ 0 & 0 & w_{11} & -w_{12} \\ 0 & 0 & -w_{12} & w_{22} \end{bmatrix}, \quad (7)$$

where A^T is a transpose of A , $Y = \text{diag}(0, \bar{n}_B + \frac{1}{2} - \frac{\eta}{2}, 0, \bar{n}_B + \frac{1}{2} - \frac{\eta}{2})$, $X = \text{diag}(1, \sqrt{\eta}, 1, \sqrt{\eta})$, and

$$w_{11} = \bar{n}_S + \frac{1}{2}, \quad (8)$$

$$w_{22} = \bar{n}_B + \eta\bar{n}_S + \frac{1}{2}, \quad (9)$$

$$w_{12} = \sqrt{\eta\bar{n}_S(\bar{n}_S + 1)}. \quad (10)$$

We now derive the QFI using the method in [41], [42]. First, the Uhlmann fidelity between zero-displacement Gaussian states $\hat{\rho}_1$ and $\hat{\rho}_2$ with covariance matrices Σ_1 and Σ_2 is [41]:

$$\mathcal{F}(\hat{\rho}_1, \hat{\rho}_2) = \frac{1}{\sqrt{\sqrt{\Gamma} + \sqrt{\Lambda}} - \sqrt{(\sqrt{\Gamma} + \sqrt{\Lambda})^2 - \Delta}}, \quad (11)$$

where the symplectic invariants are:

$$\Delta = \det(\Sigma_1 + \Sigma_2) \geq 1 \quad (12)$$

$$\Gamma = 16 \det\left(\Omega \Sigma_1 \Omega \Sigma_2 - \frac{I_{4 \times 4}}{4}\right) \geq \Delta \quad (13)$$

$$\Lambda = 16 \det\left(\Sigma_1 + \frac{j}{2}\Omega\right) \det\left(\Sigma_2 + \frac{j}{2}\Omega\right) \geq 0, \quad (14)$$

$\Omega = \begin{bmatrix} 0_{2 \times 2} & I_{2 \times 2} \\ -I_{2 \times 2} & 0_{2 \times 2} \end{bmatrix}$ is the symplectic matrix, $I_{m \times m}$ is the $m \times m$ identity matrix, and $j = \sqrt{-1}$ is the imaginary unit. The QFI is calculated as follows:

$$\mathcal{J}_{\eta, \text{TMSV}}(\bar{n}_S) \equiv \mathcal{J}_\eta(\hat{\sigma}_{IR}(\eta)) = -4 \frac{d^2 \mathcal{F}(\hat{\sigma}_{IR}(\eta), \hat{\sigma}_{IR}(\eta + \omega))}{d\omega^2} \Big|_{\omega=0} \quad (15)$$

$$= \frac{\bar{n}_S(\bar{n}_B + 1 + (1 - \eta)\bar{n}_S + \bar{n}_B\bar{n}_S)}{\eta(\bar{n}_B + 1 - \eta)(\bar{n}_B + 1 + \bar{n}_S(2\bar{n}_B + 1 - \eta))}, \quad (16)$$

where (15) is derived in [42]. Multiplying (16) by $\frac{n}{\bar{n}_S}$ and taking the limit yields the proof.² ■

Theorem 1 proves the optimality of TMSV for transmittance estimation in low photon number regime, as $\bar{n}_S \rightarrow 0$. Although it has been shown to be an optimal Gaussian state for all values of η , \bar{n}_B , and \bar{n}_S [27], characterization of a general quantum input state that maximizes QFI associated with η is an open problem. That being said, as mentioned in Section I, the low photon number per mode regime is important for the design of sensors operating under the total power constraints. Thus, we characterize and analyze a receiver structure that achieves asymptotically the quantum CRB for TMSV.

III. TRANSMITTANCE ESTIMATION USING TMSV PROBES

A. Optimal Receiver Structure

The quantum CRB for estimation of a parameter η from a quantum state $\hat{\sigma}_{IR}(\eta)$ is achieved asymptotically as the number of measurements $n \rightarrow \infty$ by the positive operator-valued measure (POVM) constructed from an eigendecomposition of the symmetric logarithmic derivative (SLD) operator $\hat{\Lambda}_\eta$. SLD is Hermitian (but not necessarily positive) and defined implicitly by [43, Ch. VIII.4(b)]:

$$\frac{\partial \hat{\sigma}_{IR}(\eta)}{\partial \eta} = \frac{1}{2} \left(\hat{\sigma}_{IR}(\eta) \hat{\Lambda}_\eta + \hat{\Lambda}_\eta \hat{\sigma}_{IR}(\eta) \right). \quad (17)$$

Since $\hat{\sigma}_{IR}(\eta)$ is Gaussian, $\hat{\Lambda}_\eta$ is a degree-2 polynomial of creation and annihilation operators \hat{a}_I , \hat{a}_R , \hat{a}_I^\dagger , and \hat{a}_R^\dagger [44, Sec. III]. Thus, there are infinitely-many unitary transformations \hat{U}_η that represent application of a finite sequence of squeezing, displacement, phase rotation, and beam splitter operators that diagonalize $\hat{\Lambda}_\eta$.

In the Appendix, we adapt approach from [17] to show that $\hat{\Lambda}_\eta = \hat{S}(\omega) (\hat{a}_I^\dagger \hat{a}_I + \hat{a}_R^\dagger \hat{a}_R) \hat{S}^\dagger(\omega)$, where $\hat{S}(\omega) = \exp(\omega^* \hat{a}_R \hat{a}_I - \omega \hat{a}_R^\dagger \hat{a}_I^\dagger)$ is a two-mode squeezing operator. Unitary $\hat{S}(\omega)$ diagonalizes $\hat{\Lambda}_\eta$ in the two-mode Fock (photon number) basis $\{|km\rangle\} \equiv |k\rangle \otimes |m\rangle$, $k, m = 0, 1, \dots$ since this is an eigenbasis for $\hat{a}_I^\dagger \hat{a}_I + \hat{a}_R^\dagger \hat{a}_R$. Thus, $\{\hat{S}(\omega) |km\rangle : k, m = 0, 1, \dots\}$ is an eigendecomposition of $\hat{\Lambda}_\eta$. Hence, an asymptotically-optimal receiver for TMSV

²Our expression for the QFI of TMSV in (16) is exact, unlike [26, Eq. (6)] and [21, Eq. (23)]. In fact, all of the QFI expressions in [26] are approximations at $\eta_a = 0$, where $\eta_a = \sqrt{\eta}$ is the amplitude transmittance, and [21, Eq. (23)] is [26, Eq. (6)] reparametrized from η_a to η . Reparametrizing (16) to η_a and setting $\eta_a = 0$ yields [26, Eq. (6)]. That a crude approximation with a zeroth-order Taylor series term yields such a close result is striking.

transmitter is a two-mode squeezer followed by the photon-number resolving (PNR) detectors on each output mode. Formally, it is the POVM $\mathcal{M} = \{\hat{M}_{km}\hat{M}_{km}^\dagger\}$, where $\hat{M}_{km} = \hat{S}(\omega)|km\rangle$. POVM \mathcal{M} followed by the maximum likelihood estimation (MLE) of η from the classical outcome of PNR detectors achieves the quantum CRB as $n \rightarrow \infty$. The squeezing parameter $\omega = \lambda - \zeta$, where ζ and λ are functions of η , \bar{n}_B , and \bar{n}_S defined in (50) and (120), respectively. We emphasize that, although our measurement is convenient in that it can be physically implemented using well-known optical elements (squeezer and PNR detectors), it is only *one of the infinitely-many* measurements that achieve quantum CRB.

B. Remarks and Caveats

The structure of our receiver is remarkable in several ways:

- It achieves quantum CRB by measuring each returned state independently, as opposed to requiring a joint measurement that entangles many returned states. While synchronization is required between returned signal and retained reference modes, this is a substantially less complicated task than performing a joint measurement.
- Optical elements implementing a two-mode squeezer required for the receiver are well-known and have been demonstrated in the laboratory [45].
- The receiver is close-to-optimal at very low input photon numbers. Our Monte-Carlo simulation described in Section V demonstrates that at moderate amount of thermal noise ($\bar{n}_B \approx 1$ photon/mode), nine photons is the sufficient resolution for PNR detectors. Such detectors, while technically complex, have been demonstrated [46].

This supports the use of our receiver, especially in applications requiring low input photon number, such as covert/LPD sensing. However, two caveats are in order:

1) *Value of ω depends on η :* The dependence of the structure of a quantum CRB-achieving measurement on the parameter of interest is a common occurrence in quantum estimation theory. It is addressed by following two-stage approach: first, obtain a rough estimate $\check{\eta}_0$ using n^β , $\beta \in (\frac{1}{2}, 1)$, probes. Then, employ $\check{\eta}_0$ to construct $\hat{S}(\omega)$ and refine $\check{\eta}$ using the remaining $n - n^\beta$ probes. This method achieves quantum CRB asymptotically using a vanishing fraction of probes [36], [37], [38, Ch. 6.4] and we use it in our Monte-Carlo simulation described in Section V.

2) *Existence of ω depends on η , \bar{n}_S , and \bar{n}_B :* The eigenbasis of the SLD $\hat{\Lambda}_\eta$ in the form $\{\hat{S}(\omega)|km\rangle : k, m = 0, 1, \dots\}$ requires the constants λ , F' , τ_1 , τ_2 to be real. Thus, per (116)-(116), we must have:

$$(C + D)^2 < 4E^2, \quad (18)$$

where C , D , and E are defined in (98)-(100). As Fig. 2 illustrates, (18) does not hold for a certain range of system parameters η , \bar{n}_S , and \bar{n}_B . Therefore, another, likely more complicated, receiver structure is necessary to realize the full quantum advantage that the TMSV states yield.³

³In the Appendix we adapt the approach in [17], where the authors derive a quantum CRB-achieving receiver for transmittance sensing when $\bar{n}_T = 0$. That receiver similarly does not exist for certain ranges of \bar{n}_S and η .

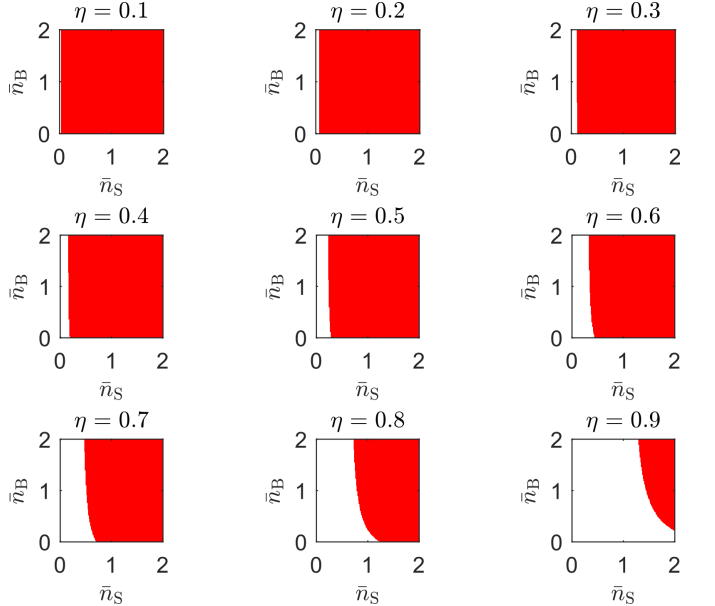


Fig. 2. Satisfaction of condition in (18) for the existence of the receiver employing two-mode squeezing followed by photon counting at various values of system parameters η , \bar{n}_S , and \bar{n}_B . Red shading denotes the regions where (18) is not satisfied, while the regions where (18) is satisfied.

Notwithstanding these caveats, the range of operating parameters that our proposed receiver covers corresponds to the low input photon number regime ($\bar{n}_S \ll 1$) which has significant practical applications (e.g., in covert/LPD or battery-constrained scenarios). It is also the regime where TMSV states are quantum-optimal. Nonetheless, we analyze and compare alternative transmittance sensing approaches next.

IV. COMPARISON WITH ALTERNATIVE TRANSMITTANCE SENSING METHODS: FUNDAMENTAL LIMITS

We compare the classical and quantum Fisher information (CFI and QFI) associated with transmittance η for several well-known receivers with the QFI for TMSV state derived in Section II and the ultimate upper bound (1) from [21].

A. Coherent Transceiver

Single-mode coherent state $|\alpha\rangle$ is an eigenstate of the annihilation operator \hat{a} and a quantum-mechanical description of laser light. There are two types of coherent detection: optical homodyne detection implements measurement along either \hat{p} or \hat{q} quadrature and yields a single Gaussian random variable (r.v.) while heterodyne detection measures both \hat{p} and \hat{q} and outputs a pair of independent Gaussian r.v.'s. A coherent transceiver employs both coherent states and detector, and is called “classical” in the literature. The QFI associated with transmittance η for a coherent state $|\alpha\rangle_S$ probe is [21, Eq. (23)]:

$$\mathcal{J}_{\eta, \text{Coh}}(\bar{n}_S) \equiv \mathcal{J}_\eta(\mathcal{E}_{S \rightarrow R}^{\bar{n}_T, \eta} [|\alpha\rangle \langle \alpha|_S]) = \frac{\bar{n}_S}{\eta(2\bar{n}_B + 1)}, \quad (19)$$

where the input mean photon number $\bar{n}_S \equiv |\alpha|^2$. A homodyne receiver achieves the corresponding quantum CRB.

B. TMSV and Optical Parametric Amplifier (OPA) Receiver

Suppose we use the TMSV probes as in Section II, but apply an optical parametric amplifier (OPA) to the output state $\hat{\sigma}_{IR}(\eta)$ instead of a two-mode squeezer. The output of the OPA is then a zero-mean thermal state with average photon number [24, Sec. A.1]:

$$\bar{n}_{\text{OPA}} = G\bar{n}_S + (G-1)(\bar{n}_B + 1 + \eta\bar{n}_S) + 2\sqrt{G(G-1)\eta\bar{n}_S(\bar{n}_S+1)}, \quad (20)$$

where the OPA gain $G > 1$. PNR detector then outputs a random photon count K distributed geometrically with mass function $q_K(k; \bar{n}_{\text{OPA}})$ defined in (3). OPA receiver was proposed for target detection with quantum illumination [24], [47], however, it can also be used to estimate transmittance η . CFI associated with η in K is:

$$\mathcal{J}_{\eta, \text{OPA}}(\bar{n}_S) = \max_{G>1} \frac{\left((G-1)\bar{n}_S + \sqrt{\frac{G(G-1)\bar{n}_S(\bar{n}_S+1)}{\eta}} \right)^2}{\bar{n}_{\text{OPA}}(\bar{n}_{\text{OPA}}+1)}. \quad (21)$$

For fixed $\bar{n}_S > 0$, the constrained maximization over gain G is challenging analytically. However, numerical approaches are tractable, and we use them to plot FI for OPA receiver in Figure 3. The dependence of optimal G on η can be addressed using the two-stage estimation approach described in Section III-B; we employ it in the Monte-Carlo simulation described in Section V. Furthermore, when \bar{n}_S is small, we have:

$$\left. \frac{\mathcal{J}_{\eta, \text{OPA}}(\bar{n}_S)}{\bar{n}_S} \right|_{\bar{n}_S=0} = \max_{G>1} \frac{G}{\eta(\bar{n}_B+1)(G(1+\bar{n}_B)-\bar{n}_B)} \quad (22)$$

$$= \frac{1}{\eta(\bar{n}_B+1)}, \quad (23)$$

where (22) is maximized when $G \rightarrow 1$. This shows that the TMSV+OPA combination can perform close to the limit in (1) in the low-SNR low-transmittance regime.

C. Fock States

It is well-known that Fock state $|m\rangle$ is optimal for transmittance sensing in vacuum ($\bar{n}_B = 0$), achieving QFI $\mathcal{J}_\eta(\mathcal{E}_{S \rightarrow R}^{0,\eta} [|m\rangle \langle m|_S]) = \frac{m}{\eta(1-\eta)}$ [18]. Here we show that this breaks down in thermal noise. The output state $\hat{\nu}_R(\eta, m) = \mathcal{E}_{S \rightarrow R}^{\bar{n}_T, \eta} [|m\rangle \langle m|_S]$ is diagonal in Fock basis, making PNR measurement optimal. The mass function for random variable K describing the photon count is derived in [48, Sec. 7.3.1]. Transformation of [48, Eq. (7.37)] using [49, 9.131.1] yields:

$$p_K(k; m) = \binom{m+k}{k} \frac{(\bar{n}_B + 1 - \eta)^{m-k} \eta^k}{(\bar{n}_B + 1)^{m+k+1}} \times {}_2F_1 \left[\begin{matrix} -k, -k \\ -(m+k) \end{matrix} ; z(\eta, \bar{n}_B) \right], \quad (24)$$

where $z(\eta, \bar{n}_B) = \frac{(\eta - \bar{n}_B)(\bar{n}_B + 1)}{\eta}$ and

$${}_2F_1 \left[\begin{matrix} a, b \\ c \end{matrix} ; z \right] = 1 + \frac{ab}{c} z + \frac{a(a+1)b(b+1)}{c(c+1)2!} z^2 + \dots \quad (25)$$

is the hypergeometric series. The QFI associated with η is:

$$\begin{aligned} \mathcal{J}_{\eta, \text{Fock}}(|m\rangle) &\equiv \mathcal{J}_\eta(\hat{\nu}_R(\eta, m)) \\ &= m \left(\frac{1-\eta}{(\bar{n}_B + 1 - \eta)^2} + \frac{1}{\eta} \right) \\ &\quad - \bar{n}_B \left(\frac{1}{(\bar{n}_B + 1 - \eta)^2} - \frac{1}{\eta^2} \right) \\ &\quad - \frac{2\bar{n}_B(\eta m + \bar{n}_B + 1)}{(\bar{n}_B + 1 - \eta)\eta^2} \\ &\quad - \frac{2\bar{n}_B^2(2(\eta m + \bar{n}_B + \eta m \bar{n}_B) + \bar{n}_B^2 + 1)}{(\bar{n}_B + 1 - \eta)^2 \eta^2} \\ &\quad - \frac{\bar{n}_B^2 m(m-1)}{(\bar{n}_B + 1 - \eta)^2} + R_m(\eta, \bar{n}_B), \end{aligned} \quad (26)$$

where

$$\begin{aligned} R_m(\eta, \bar{n}_B) &= \sum_{k=0}^{\infty} \binom{m+k}{k} \frac{k^4 \bar{n}_B^2 (\bar{n}_B + 1 - \eta)^{m-k} \eta^{k-4}}{(m+k)^2 (\bar{n}_B + 1)^{m+k-1}} \\ &\quad \times \frac{{}_2F_1 \left[\begin{matrix} -(k-1), -(k-1) \\ -(m+k-1) \end{matrix} ; z(\eta, \bar{n}_B) \right]^2}{{}_2F_1 \left[\begin{matrix} -k, -k \\ -(m+k) \end{matrix} ; z(\eta, \bar{n}_B) \right]}. \end{aligned} \quad (27)$$

The ratio of the hypergeometric series in (27) make challenging both the analysis and numerical evaluation of the QFI $\mathcal{J}_{\eta, \text{Fock}}(|m\rangle)$ for large m . Furthermore, on-demand generation of Fock states $|m\rangle$ for arbitrary m presents technical challenges that appear insurmountable in the near term. However, such sources exist for single photons [50]–[52]. Setting $m = 1$ in (24) yields

$$p_K(k; 1) = (\bar{n}_B(\bar{n}_B + 1) + \eta(k - \bar{n}_B)) \bar{n}_B^{k-1} (\bar{n}_B + 1)^{-(k+2)}. \quad (28)$$

The corresponding QFI is

$$\mathcal{J}_{\eta, \text{Fock}}(|1\rangle) = \sum_{k=0}^{\infty} \frac{(k - \bar{n}_B)^2 \bar{n}_B^{k-1} (\bar{n}_B + 1)^{-(k+2)}}{(\bar{n}_B(\bar{n}_B + 1) + \eta(k - \bar{n}_B))}. \quad (29)$$

We note that, for $\bar{n}_B > 0$, (29) is well-approximated by the first three terms of the sum: the contribution from terms corresponding to $k > 2$ decreases rapidly due to the exponential decay of $\bar{n}_B^{k-1} (\bar{n}_B + 1)^{-(k+2)}$ with increasing k .

D. TMSV and Heralded PNR Detection

TMSV states and PNR detectors can be used for probabilistic generation of Fock states: detection of m photons on the idler mode heralds $|m\rangle_S$ state on the signal mode. Thus, we consider transmittance sensing with TMSV using two directly-connected PNR detectors: one to the idler mode, and the other to the returned signal port. The CFI of this system is

$$\mathcal{J}_{\eta, \text{Her}}(\bar{n}_S) = E_M [\mathcal{J}_{\eta, \text{Fock}}(|M\rangle)], \quad (30)$$

where the output photon number M mass function is in (3).

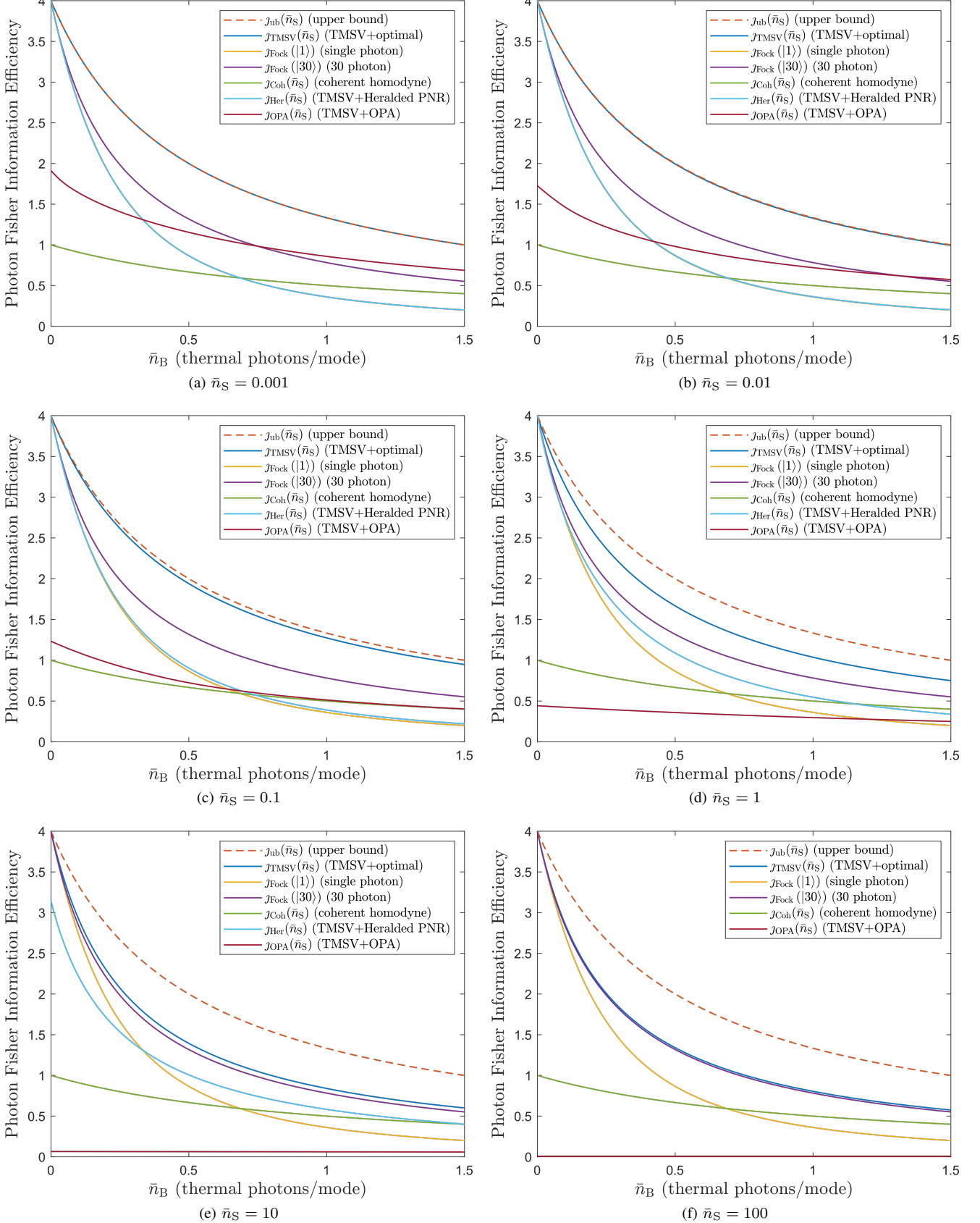


Fig. 3. Photon Fisher information efficiency vs. thermal noise level for various transmittance estimation methods and values of input photon number \bar{n}_S . We set $\eta = 0.5$, results for other values of η are qualitatively similar.

E. Comparison

We ensure fair comparison of the fundamental limits for various transmittance sensing methods by analyzing their Fisher information attained per photon per (transmitted) mode. That is, *photon Fisher information efficiency* (PFIE) $\mathcal{J}(\bar{n}_S) \equiv \frac{\mathcal{J}_\eta(\bar{n}_S)}{\bar{n}_S}$ is our figure of merit, where $\mathcal{J}_\eta(\bar{n}_S)$ is CFI or QFI attainable with \bar{n}_S input mean signal photons per mode. The ultimate upper bound for PFIE is derived from (1):

$$\mathcal{J}_{\text{ub}}(\bar{n}_S) \equiv \frac{\mathcal{J}_{\eta, \text{ub}}(\bar{n}_S)}{\bar{n}_S} = \frac{1}{\eta(\bar{n}_B + 1 - \eta)}. \quad (31)$$

The PFIE for TMSV source uses the QFI expression (16):

$$\begin{aligned} \mathcal{J}_{\text{TMSV}}(\bar{n}_S) &\equiv \frac{\mathcal{J}_{\eta, \text{TMSV}}(\bar{n}_S)}{\bar{n}_S} \\ &= \frac{\bar{n}_B + 1 + (1 - \eta)\bar{n}_S + \bar{n}_B\bar{n}_S}{\eta(\bar{n}_B + 1 - \eta)(\bar{n}_B + 1 + \bar{n}_S(2\bar{n}_B + 1 - \eta))}. \end{aligned} \quad (32)$$

The PFIE for coherent and TMSV+OPA transceivers use CFI expressions (19) and (21), respectively:

$$\mathcal{J}_{\text{Coh}}(\bar{n}_S) \equiv \frac{\mathcal{J}_{\eta, \text{Coh}}(\bar{n}_S)}{\bar{n}_S} = \frac{1}{2\eta(\bar{n}_B + 1)} \quad (33)$$

$$\begin{aligned} \mathcal{J}_{\text{OPA}}(\bar{n}_S) &\equiv \frac{\mathcal{J}_{\eta, \text{OPA}}(\bar{n}_S)}{\bar{n}_S} \\ &= \max_{G > 1} \frac{\left((G - 1)\bar{n}_S + \sqrt{\frac{G(G-1)\bar{n}_S(\bar{n}_S+1)}{\eta}}\right)^2}{\bar{n}_S\bar{n}_{\text{OPA}}(\bar{n}_{\text{OPA}} + 1)}. \end{aligned} \quad (34)$$

The PFIE for Fock state and TMSV+Heralded PNR detector use QFI and CFI expressions in (26) and (30), respectively:

$$\mathcal{J}_{\text{Fock}}(|m\rangle) \equiv \frac{\mathcal{J}_{\eta, \text{Fock}}(|m\rangle)}{m} \quad (35)$$

$$\mathcal{J}_{\text{Her}}(\bar{n}_S) \equiv \frac{\mathcal{J}_{\eta, \text{Her}}(\bar{n}_S)}{\bar{n}_S}. \quad (36)$$

We evaluate (31)-(36) and plot the results versus mean thermal noise photon number \bar{n}_B in Figure 3. While $\mathcal{J}_{\text{ub}}(\bar{n}_S)$ and $\mathcal{J}_{\text{Coh}}(\bar{n}_S)$ are constant relative to mean input photon number \bar{n}_S , $\mathcal{J}_{\text{TMSV}}(\bar{n}_S)$, $\mathcal{J}_{\text{OPA}}(\bar{n}_S)$, and $\mathcal{J}_{\text{Her}}(\bar{n}_S)$ are not. Thus, we include plots for various values of \bar{n}_S . We set $\eta = 0.5$; and note that for other values η , the plots are qualitatively similar. In plotting $\mathcal{J}_{\text{OPA}}(\bar{n}_S)$ we maximize (34) over $G > 1$ numerically. We include the plot for $\mathcal{J}_{\text{Fock}}(|m\rangle)$ for single-photon state $|1\rangle$ and a thirty-photon state $|30\rangle$ on all plots. The challenges associated with computing the hypergeometric series ${}_2F_1$ [53] precluded evaluating $\mathcal{J}_{\text{Fock}}(|m\rangle)$ for $m > 30$. Furthermore, when evaluating $\mathcal{J}_{\text{Her}}(\bar{n}_S)$ we had to truncate the sum in the expectation in (30) at $m = 30$. This accurately approximates $\mathcal{J}_{\text{Her}}(\bar{n}_S)$ only up to $\bar{n}_S \approx 4$. Thus, we did not evaluate $\mathcal{J}_{\text{Her}}(\bar{n}_S)|_{\bar{n}_S=100}$.

It is evident from Figure 3 that PFIE of the TMSV input coupled with the optimal detection exceeds that of other receivers we consider. While Fock state transmitters' performance rapidly decays with noise, they outperform the TMSV+OPA transceiver in the high-SNR regimes. Indeed, TMSV+OPA transceiver performs very poorly when input photon number is high.

On the other hand, the high photon Fisher information efficiency of single-photon state $|1\rangle$ in low noise shows the promise of the on-demand single-photon sources and PNR detection for transmittance sensing. Furthermore, since the first three terms of the summation in (29) approximate $\mathcal{J}_\eta(\bar{n}_B(\eta, 1))$ well for $\bar{n}_B < 1$, a detector that distinguishes zero, one, or more than one photons suffices for accurate estimation of η for these systems. Such detectors are less complex than full PNR detectors.

We also note that TMSV+heralded PNR performs as well as the single-photon source in low-noise setting. In fact, our calculations suggest that, for $\bar{n}_S \ll 1$, TMSV+heralded PNR detector matches PFIE of a single-photon source while using a less-complex single-photon detector (SPD) that distinguishes zero or more than zero photons instead of a PNR detector.

Nevertheless, many practical scenarios demand low-input power operation. Even for moderate noise power levels, this results in low SNR. TMSV+receiver derived in Section III and TMSV+OPA receiver behave well in this setting. Thus, Monte-Carlo simulation that we discuss next evaluates the convergence as number of probes n increases of the mean-squared error to the corresponding Cramér-Rao bounds for maximum-likelihood estimators that use outputs of these receiver as well as a coherent transceiver.

V. COMPARISON WITH ALTERNATIVE TRANSMITTANCE SENSING METHODS: SIMULATIONS

Maximum likelihood estimators (MLEs) have a number of desirable properties, first and foremost being the availability of “turn-the-crank” implementation in most practical settings. Furthermore, MLE is asymptotically consistent (converges in probability to the value being estimated) and efficient (achieves CRB) as number of observations $n \rightarrow \infty$ [6], [54]. Here we employ MLE to estimate transmittance η from the outputs of coherent homodyne transceiver, TMSV+OPA receiver, and TMSV+receiver derived in Section III, analyzing their convergence to CRB for increasing n .

A. Construction of MLEs

1) *Coherent Homodyne Transceiver*: Suppose a product $|\alpha\rangle_S^{\otimes n}$ of n coherent states $|\alpha\rangle_S$ with $\alpha = \sqrt{\bar{n}_S}$ is input as probes. The corresponding output of a homodyne receiver is a sequence of n independent and identically distributed (i.i.d.) Gaussian random variables $\{X_k\}_{k=1}^n$, each with mean $\sqrt{\eta\bar{n}_S}$ and variance $\bar{n}_B + 1$. The MLE for η is:

$$\hat{\eta}_{\text{Coh}}(n) = \frac{1}{\bar{n}_S} \left(\sum_{k=1}^n x_k \right)^2, \quad (37)$$

where x_k is an observed instance of X_k .

2) *TMSV Input and OPA Receiver*: Now suppose a product $\hat{\rho}_{I^n S^n} = |\psi\rangle \langle \psi|_{IS}^{\otimes n}$ of TMSV states defined in (2) is used as input. The corresponding output of an OPA receiver is a sequence of n i.i.d. geometric random variables $\{Y_k\}_{k=1}^n$,

each with mass function $q_Y(y; \bar{n}_{\text{OPA}})$ defined in (3), where the \bar{n}_{OPA} is given in (20). The MLE for η is:

$$\check{\eta}_{\text{OPA}}(n) = \frac{\bar{y}(G^* - 1) - 1 - \bar{n}_B}{(G^* - 1)^2 \bar{n}_S} - \frac{2\sqrt{G^*(1 + \bar{y} + \bar{n}_B - G^*\bar{n}_S)(1 + \bar{n}_S)}}{(G^* - 1)\bar{n}_S} + \frac{G^*(G^* + 2\bar{n}_B - G^*\bar{n}_B + (G^* - 1)\bar{n}_S)}{(G^* - 1)^2 \bar{n}_S}, \quad (38)$$

where $\bar{y} = \frac{1}{n} \sum_{k=1}^n y_k$ is the mean of the observed instances of Y_k , and G^* is the OPA gain that maximizes CFI in (21). Thus, G^* minimizes the CRB for the receiver, and, hence, the asymptotic MSE of $\check{\eta}_{\text{OPA}}$. However, G^* depends on the parameter of interest η . Thus, we follow a two-stage approach [36], [37], [38, Ch. 6.4]: first, we obtain a preliminary estimate $\check{\eta}_0 = \check{\eta}_{\text{Coh}}(\sqrt{n})$ using coherent homodyne transceiver described above for first \sqrt{n} probes. Then, we obtain G_0^* by maximizing (21) with $\check{\eta}_0$ substituted for η . Remaining $n - \sqrt{n}$ probes are TMSV states, with output processed by the OPA receiver with gain G_0^* and the corresponding MLE $\check{\eta}_{\text{OPA}}(n - \sqrt{n})$ in (38) with G^* set to G_0^* .

3) TMSV Input and Receiver Derived in Section III:

Suppose a product $\hat{\rho}_{I^n S^n} = |\psi\rangle \langle \psi|_{IS}^{\otimes n}$ of TMSV states defined in (2) is used as input, but we employ the receiver derived in Section III that uses two-mode squeezer $\hat{S}(\omega)$ followed by photon number measurement of each mode. As noted in Section III-B, the squeezing parameter ω depends on the parameter of interest η . We follow a two-stage approach as we do for construction of the OPA receiver, with an identical first stage that uses a coherent homodyne transceiver. The resulting preliminary estimate $\check{\eta}_0$ that uses the first \sqrt{n} probes is employed to find the squeezing parameter ω_0 . Remaining $n - \sqrt{n}$ probes are TMSV states, with each output state $\hat{\sigma}_{IR}(\eta)$ processed by $\hat{S}(\omega_0)$ followed by a two-mode photon number measurement. Thus, the corresponding output is a sequence of n i.i.d. pairs of random variables $\{(Z_{0,k}, Z_{1,k})\}_{k=1}^n$, each with mass function:

$$p_{Z_0, Z_1}(z_0, z_1) = \langle z_0 z_1 | \hat{S}^\dagger(\omega_0) \hat{\sigma}_{IR}(\eta) \hat{S}(\omega_0) | z_0 z_1 \rangle \quad (39)$$

$$= \sum_{s,t} r_{st} \left| \langle st | \hat{S}(\omega_0 + \zeta) | z_0 z_1 \rangle \right|^2, \quad (40)$$

where [55, Eq. (22)]:

$$\begin{aligned} & \langle st | \hat{S}(\omega_0 + \zeta) | z_0 z_1 \rangle \\ &= \sum_{u=0}^{u_e} \sum_{l=0}^{l_e} \frac{\delta_{z_0+t, z_1+s} \tau_0 s_{ul}^{(1)} \sqrt{z_0! z_1!} s! t! e^{(\omega_0 + \zeta) s_{ul}^{(2)}}}{u! (z_0 - u)! (z_1 - u)! (s - l)! l! (s - l)! (t - l)!}, \end{aligned}$$

with $u_e = \min(z_0, z_1)$, $l_e = \min(s, t)$, $\tau_0 = (-1)^{u+l} (\text{sech}(\omega_0 + \zeta))^{s_{ul}^{(1)} + 1}$, $s_{ul}^{(1)} = z_1 + s - u - l + 1$, $s_{ul}^{(2)} = u - l + s - z_0$, and ζ and r_{st} defined in (50) and (58), respectively. Since there is no known closed-form solution for MLE, we construct it using numerical optimization of (39) recast as a likelihood function for η .

B. Results

While it is well-known that MLE is asymptotically consistent and efficient as number of observations $n \rightarrow \infty$ [6],

[54], numerical approaches are needed for its *finite sample* performance analysis at fixed $n < \infty$. Furthermore, although the two-stage approach is consistent and efficient as $n \rightarrow \infty$ [36], [37], [38, Ch. 6.4], to our knowledge, its finite sample analysis is missing from the literature.

We address this by comparing the simulated MSEs for the MLEs developed in Section V-A to their corresponding CRBs. Our settings for $\bar{n}_S = 0.01$, $\bar{n}_B = 1$, and $\eta = 0.5$ are chosen because 1) they model a practical scenario of transmittance sensing in contested environment; 2) they allow the simulations to complete in reasonable time; and, 3) they ensure the existence of the receiver derived in Section III. MSE is inversely proportional to number of observations n (here n is the number of modes used to estimate η): $\text{MSE}_\eta = \frac{c_\eta}{n}$. For \bar{n}_S , \bar{n}_B , and η fixed, the scaling factor $c_\eta \equiv n \times \text{MSE}_\eta$ is a function of n , however, the asymptotic efficiency of MLE implies that, for estimators described in Section V-A, $\lim_{n \rightarrow \infty} c_\eta = \frac{1}{\mathcal{J}_\eta}$, where $\frac{1}{\mathcal{J}_\eta}$ is a single-observation CRB. We are interested in the speed of c_η 's convergence to $\frac{1}{\mathcal{J}_\eta}$ as n increases, and the penalty (if any) of the two-stage approach.

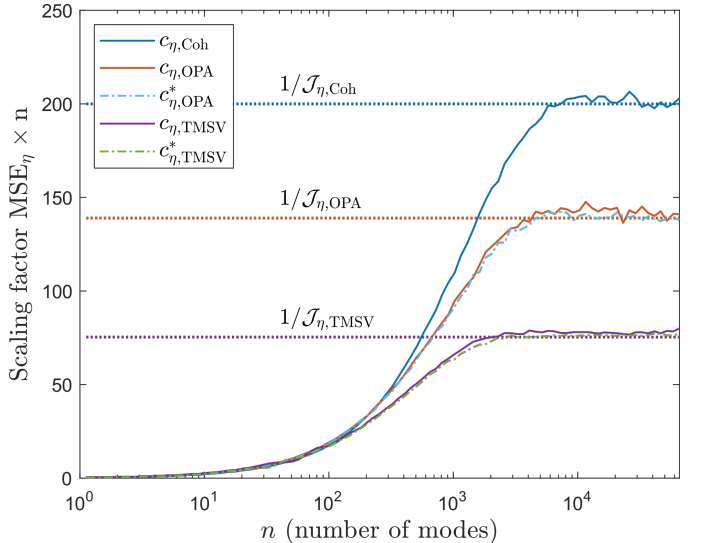


Fig. 4. Scaling factor $c_\eta = n \times \text{MSE}_\eta$ vs. number of modes n used to estimate η . We set $\bar{n}_S = 0.01$, $\bar{n}_B = 1$, and $\eta = 0.5$. We evaluate c_η at 96 logarithmically-spaced values for $n \in [1, 65536]$; limitations of machine precision, computational run-time, and memory precluded evaluation of c_η for $n > 65536$. Each data point is an average of 5×10^4 results from Monte Carlo simulations. The 95% confidence intervals are negligibly small; the fluctuations in the plots are due to machine precision limits rather than stochastic variations between experiments.

On the ordinate in Figure 4 we plot the scaling factors $c_{\eta,\text{Coh}}$, $c_{\eta,\text{OPA}}$, and $c_{\eta,\text{TMSV}}$ for the MLEs that use the output of coherent homodyne transceiver, TMSV+OPA receiver, and TMSV+receiver derived in Section III, respectively. We also plot the scaling factors $c_{\eta,\text{OPA}}^*$ and $c_{\eta,\text{TMSV}}^*$ for the corresponding receivers constructed with knowledge of η . While such receivers cannot physically exist, this enables us to isolate the impact of the two-stage method on the convergence of the scaling factor.

Figure 4 shows that $c_{\eta,\text{TMSV}}$ converges to $\frac{1+e_{\text{two-stage}}}{\mathcal{J}_{\eta,\text{TMSV}}(\bar{n}_S)}$ at approximately $n = 3000$ modes, $c_{\eta,\text{OPA}}$ converges to $\frac{1+e_{\text{two-stage}}}{\mathcal{J}_{\eta,\text{OPA}}(\bar{n}_S)}$ at approximately $n = 5000$ modes, $c_{\eta,\text{Coh}}$ converges to

$\frac{1}{\mathcal{J}_{\eta, \text{Coh}}(\bar{n}_S)}$ at approximately $n = 8000$ modes. The penalty from the use of the two-stage method $e_{\text{two-stage}} \approx 0.05$, and appears to decay with n . We note that $\frac{1}{\mathcal{J}_{\eta, \text{TMSV}}(\bar{n}_S)}$ is negligibly close to the ultimate lower bound $\frac{1}{\mathcal{J}_{\eta, \text{ub}}(\bar{n}_S)}$.

Finally, for $\bar{n}_S = 0.01$, $\bar{n}_B = 1$, and $\eta = 0.5$, the required squeezing parameter in the receiver we derived in Section III is $\omega \approx 0.1428$. This corresponds to only -8.4541 dB of squeezing, and is substantially less than 10 dB that has been demonstrated at 1550 nm “telecom” wavelength [45]. Furthermore, we approximate the ideal PNR by one that resolves up to 9 photons, which captures > 99% of the probability mass in (39). Such resolution has been demonstrated at 1550 nm using superconducting transition-edge sensors [46]. For the OPA receiver, the optimal gain $G^* = 1.154$. OPA receiver has been used in quantum illumination experiments [47]. Although there are many technical challenges, such as idler mode storage and synchronization, this supports the feasibility of near-future experimental validation of our work.

VI. DISCUSSION

We showed that the TMSV state asymptotically minimizes the quantum CRB for loss estimation in thermal noise and low input photon number regime over all states (not necessarily Gaussian). To our knowledge, this is the first example of a substantial performance gain from quantum illumination outside the high-noise low-SNR regime. We derived a quantum CRB-achieving receiver structure for TMSV source: a two-mode squeezer followed by the PNR detection. Although our design is restricted to a certain range of parameters, the range corresponds to the low input photon number regime where TMSV source achieves the ultimate QFI bound in (1). Nevertheless, alternate receiver structures for TMSV input that are not restricted to this range of parameters should be explored. The structure of our receiver depends on the parameter of interest, as is typical in quantum-enhanced sensing. This necessitates a two-stage estimation approach [36], [37], [38, Ch. 6.4], however, our simulations strongly suggest that its impact on the MSE is negligible. Thus, our work shows promise for future experiment demonstrating quantum advantage in loss sensing.

APPENDIX

We adapt the approach from [17] to obtain a quantum CRB-achieving receiver for transmittance when $\bar{n}_T = 0$. We derive an eigendecomposition $\{\hat{S}(\omega) |km\rangle : k, m = 0, 1, \dots\}$ of $\hat{\Lambda}_\eta$ in three steps: 1) we find an orthonormal basis $\{|\psi_{km}\rangle\}$, $k, m = 0, 1, \dots$ for the output state $\hat{\sigma}_{IR}(\eta)$; 2) we use $\{|\psi_{km}\rangle\}$ to write $\hat{\Lambda}_\eta$ as a linear combination of creation and annihilation operators \hat{a}_I , \hat{a}_R , \hat{a}_I^\dagger , and \hat{a}_R^\dagger of the return and idler modes; and, 3) we recognize that the resulting linear combination is produced by an action of a two-mode squeezing operator $\hat{S}(\omega)$ on a number operator, yielding an expression for ω .

A. Orthonormal Basis for the Output State $\hat{\sigma}_{IR}(\eta)$

Squeezing the two modes of $\hat{\sigma}_{IR}(\eta)$ yields $\hat{\sigma}_{IR}^d = \hat{S}(\zeta)\hat{\sigma}_{IR}\hat{S}^\dagger(\zeta)$ with the covariance matrix:

$$\Sigma_{\hat{\sigma}_{IR}^d} = Z \Sigma_{\hat{\sigma}_{IR}(\eta)} Z^T \quad (41)$$

$$= \begin{bmatrix} w_1^d & w_{12}^d & 0 & 0 \\ w_{12}^d & w_2^d & 0 & 0 \\ 0 & 0 & w_1^d & -w_{12}^d \\ 0 & 0 & -w_{12}^d & w_2^d \end{bmatrix}, \quad (42)$$

where

$$Z = \begin{bmatrix} \cosh(\zeta) & \sinh(\zeta) & 0 & 0 \\ \sinh(\zeta) & \cosh(\zeta) & 0 & 0 \\ 0 & 0 & \cosh(\zeta) & -\sinh(\zeta) \\ 0 & 0 & -\sinh(\zeta) & \cosh(\zeta) \end{bmatrix} \quad (43)$$

$$w_1^d = w_1 \cosh^2(\zeta) + w_2 \sinh^2(\zeta) + w_{12} \sinh(2\zeta), \quad (44)$$

$$w_2^d = w_2 \cosh^2(\zeta) + w_1 \sinh^2(\zeta) + w_{12} \sinh(2\zeta), \quad (45)$$

$$w_{12}^d = w_{12} \cosh(2\zeta) + (w_1 + w_2) \cosh(\zeta) \sinh(\zeta). \quad (46)$$

A value of ζ such that

$$w_{12}^d = 0 \quad (47)$$

makes $\hat{\sigma}_{IR}^d(\eta)$ a thermal state that is diagonal in the Fock basis. Note that in (46), $w_1 > 0$, $w_2 > 0$, $w_{12} > 0$ and $\cosh(\zeta) > 0$. Thus, $\sinh(\zeta) < 0$. Solution of (47) for ζ under these constraints satisfies:

$$\cosh(\zeta) = \sqrt{\frac{1}{2} + \frac{1 + \bar{n}_B + \bar{n}_S + \bar{n}_S \eta}{2\sqrt{a}}} \equiv \mu, \quad (48)$$

$$\sinh(\zeta) = -\sqrt{-\frac{1}{2} + \frac{1 + \bar{n}_B + \bar{n}_S + \bar{n}_S \eta}{2\sqrt{a}}} \equiv \nu. \quad (49)$$

This yields, in turn,

$$\zeta = -\log \left(\sqrt{\frac{1}{2} + \sqrt{\frac{1}{2} + \frac{1 + \bar{n}_B + \bar{n}_S + \bar{n}_S \eta}{2\sqrt{a}}}} \right. \\ \left. + \sqrt{-\frac{1}{2} + \sqrt{\frac{1}{2} + \frac{1 + \bar{n}_B + \bar{n}_S + \bar{n}_S \eta}{2\sqrt{a}}}} \right) \quad (50)$$

$$w_1^d = \frac{1}{2} (-\bar{n}_B + \bar{n}_S(1 - \eta) + \sqrt{a}) \quad (51)$$

$$w_2^d = \frac{1}{2} (\bar{n}_B - \bar{n}_S(1 - \eta) + \sqrt{a}), \quad (52)$$

where

$$a = \bar{n}_B^2 + (1 + \bar{n}_S(1 - \eta))^2 + 2\bar{n}_B(1 + \bar{n}_S + \bar{n}_S \eta). \quad (53)$$

The covariance matrix of $\hat{\sigma}_{IR}^d$ can be expressed as

$$\Sigma_{\hat{\sigma}_{IR}^d(\eta)} = \begin{bmatrix} N_1 + \frac{1}{2} & 0 & 0 & 0 \\ 0 & N_2 + \frac{1}{2} & 0 & 0 \\ 0 & 0 & N_1 + \frac{1}{2} & 0 \\ 0 & 0 & 0 & N_2 + \frac{1}{2} \end{bmatrix}, \quad (54)$$

where the mean thermal photon numbers in each mode are:

$$N_1 = w_1^d - \frac{1}{2} = \frac{1}{2} (\bar{n}_B - 1 + \bar{n}_S(\eta - 1) + \sqrt{a}) \quad (55)$$

$$N_2 = w_2^d - \frac{1}{2} = \frac{1}{2} (-\bar{n}_B - 1 - \bar{n}_S(\eta - 1) + \sqrt{a}). \quad (56)$$

Hence, using two-mode Fock basis, we have:

$$\hat{\sigma}_{IR}^d(\eta) = \sum_{km} r_{km} |km\rangle \langle km|, \quad (57)$$

where, using definition of $q(k, \bar{n})$ from (3),

$$r_{km} \equiv q(k, N_1)q(m, N_2) = \frac{N_1^k N_2^m}{(1 + N_1)^{k+1}(1 + N_2)^{m+1}}. \quad (58)$$

Therefore, the output state $\hat{\sigma}_{IR}(\eta)$ is diagonal in the two-mode squeezed Fock basis $\{|\psi_{km}\rangle\}$, $k, m = 0, 1, \dots$:

$$\hat{\sigma}_{IR}(\eta) = \hat{S}^\dagger(\zeta) \hat{\sigma}_{IR}^d \hat{S}(\zeta) = \sum_{km} r_{km} |\psi_{km}\rangle \langle \psi_{km}|, \quad (59)$$

where $|\psi_{km}\rangle = \hat{S}^\dagger(\zeta) |km\rangle$ defines an orthonormal basis.

B. Actions of Modal Creation and Annihilation on Output State

Since the squeezing parameter ζ is real, we have [14, Eq. (5.35)]

$$S(\zeta) \hat{a}_R S^\dagger(\zeta) = \mu \hat{a}_R + \nu \hat{a}_I^\dagger, \quad (60)$$

$$S(\zeta) \hat{a}_R^\dagger S^\dagger(\zeta) = \mu \hat{a}_R^\dagger + \nu \hat{a}_I, \quad (61)$$

where μ and ν are defined in (48) and (49), respectively. These facts, the diagonalization of the output state $\hat{\sigma}_{IR}(\eta)$ in (59), and the photon-number raising and lowering properties of creation and annihilation operators allow us to derive the following:

$$\begin{aligned} & \langle \psi_{km} | 2\hat{a}_R \hat{\sigma}_{IR}(\eta) \hat{a}_R^\dagger | \psi_{st} \rangle \\ &= \langle km | S(\zeta) 2\hat{a}_R S^\dagger(\zeta) \sum_{ul} r_{ul} |ul\rangle \langle ul| S(\zeta) \hat{a}_R^\dagger S^\dagger(\zeta) |st\rangle \\ &= \langle km | 2(\mu \hat{a}_R + \nu \hat{a}_I^\dagger) \sum_{ul} r_{ul} |ul\rangle \langle ul| (\mu \hat{a}_R^\dagger + \nu \hat{a}_I) |st\rangle \\ &= \langle km | 2(\mu \hat{a}_R + \nu \hat{a}_I^\dagger) \sum_{ul} r_{ul} |ul\rangle \langle ul| (\mu \sqrt{r+1} |s+1, t\rangle \\ & \quad + \nu \sqrt{t-1} |s, t-1\rangle) \\ &= \langle km | 2(\mu \hat{a}_R + \nu \hat{a}_I^\dagger) (\mu r_{s+1,t} \sqrt{r+1} |s+1, t\rangle \\ & \quad + \nu r_{s,t-1} \sqrt{t-1} |s, t-1\rangle) \\ &= \langle km | 2(\mu \hat{a}_R + \nu \hat{a}_I^\dagger) (\mu r_{s+1,t} \hat{a}_R^\dagger + \nu r_{s,t-1} \hat{a}_I) |st\rangle \end{aligned} \quad (62)$$

$$\begin{aligned} & \langle \psi_{km} | \hat{a}_R^\dagger \hat{a}_R \hat{\sigma}_{IR}(\eta) | \psi_{st} \rangle \\ &= \langle km | S(\zeta) \hat{a}_R^\dagger S^\dagger(\zeta) S(\zeta) \hat{a}_R S^\dagger(\zeta) \sum_{ul} r_{ul} |ul\rangle \langle \psi_{ul} | \psi_{st} \rangle \\ &= \langle km | (\mu \hat{a}_R^\dagger + \nu \hat{a}_I) (\mu \hat{a}_R + \nu \hat{a}_I^\dagger) r_{st} |st\rangle \end{aligned} \quad (63)$$

$$\begin{aligned} & \langle \psi_{km} | \hat{\sigma}_{IR}(\eta) \hat{a}_R^\dagger \hat{a}_R | \psi_{st} \rangle \\ &= \langle \psi_{km} | \sum_{ul} r_{ul} | \psi_{ul} \rangle \langle ul | S(\zeta) \hat{a}_R^\dagger S^\dagger(\zeta) S(\zeta) \hat{a}_R S^\dagger(\zeta) |st\rangle \end{aligned} \quad (64)$$

$$\begin{aligned} &= \langle km | r_{km} (\mu \hat{a}_R^\dagger + \nu \hat{a}_I) (\mu \hat{a}_R + \nu \hat{a}_I^\dagger) |st\rangle \\ &= \langle \psi_{km} | 2\hat{a}_R^\dagger \hat{\sigma}_{IR}(\eta) \hat{a}_R | \psi_{st} \rangle \\ &= \langle km | S(\zeta) 2\hat{a}_R^\dagger S^\dagger(\zeta) \sum_{ul} r_{ul} |ul\rangle \langle ul | S(\zeta) \hat{a}_R S^\dagger(\zeta) |st\rangle \\ &= \langle km | 2(\mu \hat{a}_R^\dagger + \nu \hat{a}_I) \sum_{ul} r_{ul} |ul\rangle \langle ul | (\mu \hat{a}_R + \nu \hat{a}_I^\dagger) |st\rangle \\ &= \langle km | 2(\mu \hat{a}_R^\dagger + \nu \hat{a}_I) \sum_{ul} r_{ul} |ul\rangle \langle ul | (\mu \sqrt{k} |s-1, t\rangle \\ & \quad + \nu \sqrt{t+1} |s, t+1\rangle) \end{aligned} \quad (64)$$

$$\begin{aligned} &= \langle km | 2(\mu \hat{a}_R^\dagger + \nu \hat{a}_I) (\mu r_{s-1,t} \sqrt{k} |s-1, t\rangle \\ & \quad + \nu r_{s,t+1} \sqrt{t+1} |s, t+1\rangle) \\ &= \langle km | 2(\mu \hat{a}_R^\dagger + \nu \hat{a}_I) (\mu r_{s-1,t} \hat{a}_R + \nu r_{s,t+1} \hat{a}_I^\dagger) |st\rangle \end{aligned} \quad (65)$$

$$\begin{aligned} & \langle \psi_{km} | \hat{a}_R \hat{a}_R^\dagger \hat{\sigma}_{IR}(\eta) | \psi_{st} \rangle \\ &= \langle km | S(\zeta) \hat{a}_R S^\dagger(\zeta) S(\zeta) \hat{a}_R^\dagger S^\dagger(\zeta) \sum_{ul} r_{ul} |ul\rangle \langle \psi_{ul} | \psi_{st} \rangle \\ &= \langle km | (\mu \hat{a}_R + \nu \hat{a}_I^\dagger) (\mu \hat{a}_R^\dagger + \nu \hat{a}_I) r_{st} |st\rangle \end{aligned} \quad (66)$$

$$\begin{aligned} & \langle \psi_{km} | \hat{\sigma}_{IR}(\eta) \hat{a}_R \hat{a}_R^\dagger | \psi_{st} \rangle \\ &= \langle \psi_{km} | \sum_{ul} r_{ul} | \psi_{ul} \rangle \langle ul | S(\zeta) \hat{a}_R S^\dagger(\zeta) S(\zeta) \hat{a}_R^\dagger S^\dagger(\zeta) |st\rangle \\ &= \langle km | r_{km} (\mu \hat{a}_R + \nu \hat{a}_I^\dagger) (\mu \hat{a}_R^\dagger + \nu \hat{a}_I) |st\rangle \end{aligned} \quad (67)$$

C. Characterization of SLD $\hat{\Lambda}_\eta$

First, we use (17) to relate the $kmst$ -th term of the SLD operator $\hat{\Lambda}_\eta$ in the basis $\{|\psi_{km}\rangle\}$ to the corresponding term of the derivative $\frac{d\hat{\sigma}_{IR}(\eta)}{d\eta}$:

$$\begin{aligned} \langle \psi_{km} | \frac{d\hat{\sigma}_{IR}(\eta)}{d\eta} | \psi_{st} \rangle &= \frac{1}{2} \langle \psi_{km} | \hat{\sigma}_{IR}(\eta) \hat{\Lambda}_\eta | \psi_{st} \rangle \\ & \quad + \frac{1}{2} \langle \psi_{km} | \hat{\Lambda}_\eta \hat{\sigma}_{IR}(\eta) | \psi_{st} \rangle \end{aligned} \quad (68)$$

$$= \frac{r_{km} + r_{st}}{2} \langle \psi_{km} | \hat{\Lambda}_\eta | \psi_{st} \rangle. \quad (69)$$

Thus, the SLD operator is expressed as follows:

$$\hat{\Lambda}_\eta = \sum_{kmst} \langle \psi_{km} | \frac{2 \frac{d\hat{\sigma}_{IR}(\eta)}{d\eta}}{r_{km} + r_{st}} | \psi_{st} \rangle | \psi_{km} \rangle \langle \psi_{st}|. \quad (70)$$

The probe state evolving in a thermal bath is characterized by the Lindblad Master equation [56, Ch. 4]:

$$\frac{d\hat{\sigma}_{IR}(\eta)}{dt} = \frac{\gamma}{2} \left[(\bar{n}_B + 1) \hat{\mathcal{L}}_R[\hat{a}] + \bar{n}_B \hat{\mathcal{L}}_R[\hat{a}^\dagger] \right] \hat{\sigma}_{IR}(\eta), \quad (71)$$

where the superoperator $\hat{\mathcal{L}}_R[\cdot]$ is defined as follows:

$$\begin{aligned} \hat{\mathcal{L}}_R[\hat{a}] \hat{\sigma}_{IR}(\eta) &= 2\hat{a}_R \hat{\sigma}_{IR}(\eta) \hat{a}_R^\dagger - \hat{a}_R^\dagger \hat{a}_R \hat{\sigma}_{IR}(\eta) \\ & \quad - \hat{\sigma}_{IR}(\eta) \hat{a}_R^\dagger \hat{a}_R \end{aligned} \quad (72)$$

$$\begin{aligned} \hat{\mathcal{L}}_R[\hat{a}^\dagger] \hat{\sigma}_{IR}(\eta) &= 2\hat{a}_R^\dagger \hat{\sigma}_{IR}(\eta) \hat{a}_R - \hat{a}_R \hat{a}_R^\dagger \hat{\sigma}_{IR}(\eta) \\ & \quad - \hat{\sigma}_{IR}(\eta) \hat{a}_R \hat{a}_R^\dagger. \end{aligned} \quad (73)$$

The dissipation rate γ satisfies $\exp(-\frac{\gamma}{2}t) = \sqrt{\eta}$, which, in turn, implies:

$$\frac{dt}{d\eta} = \frac{1}{\gamma\eta}. \quad (74)$$

Employing the chain rule in (71) using (74), and substituting the result into (70) yields:

$$\hat{\Lambda}_\eta = \sum_{kmst} \langle \psi_{km} | \frac{2 \frac{d\hat{\sigma}_{IR}(\eta)}{dt} \frac{dt}{d\eta}}{r_{km} + r_{st}} | \psi_{st} \rangle | \psi_{km} \rangle \langle \psi_{st} | \quad (75)$$

$$= \frac{(\bar{n}_B + 1)}{\eta} \sum_{kmst} \frac{\langle \psi_{km} | \hat{\mathcal{L}}_R[\hat{a}] \hat{\sigma}_{IR}(\eta) | \psi_{st} \rangle}{r_{km} + r_{st}} | \psi_{km} \rangle \langle \psi_{st} | \\ + \frac{\bar{n}_B}{\eta} \sum_{kmst} \frac{\langle \psi_{km} | \hat{\mathcal{L}}_R[\hat{a}^\dagger] \hat{\sigma}_{IR}(\eta) | \psi_{st} \rangle}{r_{km} + r_{st}} | \psi_{km} \rangle \langle \psi_{st} | \quad (76)$$

We analyze the two summations in (76) separately. First,

$$\frac{\langle \psi_{km} | \hat{\mathcal{L}}_R[\hat{a}] \hat{\sigma}_{IR}(\eta) | \psi_{st} \rangle}{r_{km} + r_{st}} \\ = \frac{\langle \psi_{km} | 2\hat{a}_R \hat{\sigma}_{IR}(\eta) \hat{a}_R^\dagger | \psi_{st} \rangle}{r_{km} + r_{st}} \\ - \frac{\langle \psi_{km} | \hat{a}_R^\dagger \hat{a}_R \hat{\sigma}_{IR}(\eta) | \psi_{st} \rangle}{r_{km} + r_{st}} \\ - \frac{\langle \psi_{km} | \hat{\sigma}_{IR}(\eta) \hat{a}_R^\dagger \hat{a}_R | \psi_{st} \rangle}{r_{km} + r_{st}} \quad (77)$$

$$= \frac{\langle km | 2(\mu\hat{a}_R + \nu\hat{a}_I^\dagger)(\mu r_{s+1,t}\hat{a}_R^\dagger + \nu r_{s,t-1}\hat{a}_I) | st \rangle}{r_{km} + r_{st}} \\ - \langle km | (\mu\hat{a}_R^\dagger + \nu\hat{a}_I)(\mu\hat{a}_R + \nu\hat{a}_I^\dagger) | st \rangle \quad (78)$$

$$= \langle km | \left(\frac{2r_{s+1,t}}{r_{km} + r_{st}} - 1 \right) \mu^2 \hat{a}_R^\dagger \hat{a}_R | st \rangle \\ + \langle km | \left(\frac{2r_{s+1,t}}{r_{km} + r_{st}} - 1 \right) \nu \mu \hat{a}_I^\dagger \hat{a}_R^\dagger | st \rangle \\ + \langle km | \left(\frac{2r_{s,t-1}}{r_{km} + r_{st}} - 1 \right) \mu \nu \hat{a}_R \hat{a}_I | st \rangle \\ + \langle km | \left(\frac{2r_{s,t-1}}{r_{km} + r_{st}} - 1 \right) \nu^2 \hat{a}_I^\dagger \hat{a}_I | st \rangle \\ + \left(\frac{2\mu^2 r_{s+1,t}}{r_{km} + r_{st}} - \nu^2 \right) \langle km | st \rangle, \quad (79)$$

where μ and ν are defined in (48) and (49), respectively, (78) is derived using (62)-(67) in Appendix B, and (79) is due to the commutation relation $[\hat{a}, \hat{a}^\dagger] = 1$ and rearrangement of terms. Observe that the first, fourth, and fifth terms in (79) is not zero only when $\{k = s, m = t\}$, while the second and third terms are not zero when $\{k = s + 1, m = t + 1\}$ and $\{k = s - 1, m = t - 1\}$, respectively. Since

$$\frac{2r_{s+1,t}}{r_{km} + r_{st}} \Big|_{k=s, m=t} - 1 = -\frac{1}{1 + N_1} \quad (80)$$

$$\frac{2r_{s+1,t}}{r_{km} + r_{st}} \Big|_{k=s+1, m=t+1} - 1 = \frac{N_1 - N_2 - 1}{2N_1 N_2 + N_1 + N_2 + 1} \quad (81)$$

$$\frac{2r_{s,t-1}}{r_{km} + r_{st}} \Big|_{k=s-1, m=t-1} - 1 = \frac{N_1 - N_2 - 1}{2N_1 N_2 + N_1 + N_2 + 1} \quad (82)$$

$$\frac{2r_{s,t-1}}{r_{km} + r_{st}} \Big|_{k=s, m=t} - 1 = \frac{1}{N_2}, \quad (83)$$

with N_1 and N_2 defined in (55) and (56), respectively, we have:

$$\sum_{kmst} \frac{\langle \psi_{km} | \hat{\mathcal{L}}_R[\hat{a}] \hat{\sigma}_{IR}(\eta) | \psi_{st} \rangle}{r_{km} + r_{st}} | \psi_{km} \rangle \langle \psi_{st} | \\ = \hat{S}^\dagger(\zeta) \hat{K}_1 \hat{S}(\zeta), \quad (84)$$

where

$$\hat{K}_1 = \left(\frac{N_1 - N_2 - 1}{2N_1 N_2 + N_1 + N_2 + 1} \right) \nu \mu \left(\hat{a}_I^\dagger \hat{a}_R^\dagger + \hat{a}_R \hat{a}_I \right) \\ - \frac{\mu^2 \hat{a}_R^\dagger \hat{a}_R}{1 + N_1} + \frac{\nu^2}{N_2} \hat{a}_I^\dagger \hat{a}_I + \mu^2 \frac{N_1}{1 + N_1} - \nu^2. \quad (85)$$

Now, the $kmst$ -th term in the second summation in (76) is:

$$\frac{\langle \psi_{km} | \hat{\mathcal{L}}_R[\hat{a}^\dagger] \hat{\sigma}_{IR}(\eta) | \psi_{st} \rangle}{r_{km} + r_{st}} \\ = \frac{\langle \psi_{km} | 2\hat{a}_R^\dagger \hat{\sigma}_{IR}(\eta) \hat{a}_R | \psi_{st} \rangle}{r_{km} + r_{st}} \\ - \frac{\langle \psi_{km} | \hat{a}_R \hat{a}_R^\dagger \hat{\sigma}_{IR}(\eta) | \psi_{st} \rangle}{r_{km} + r_{st}} \\ - \frac{\langle \psi_{km} | \hat{\sigma}_{IR}(\eta) \hat{a}_R \hat{a}_R^\dagger | \psi_{st} \rangle}{r_{km} + r_{st}} \quad (86)$$

$$= \frac{\langle km | 2(\mu\hat{a}_R^\dagger + \nu\hat{a}_I)(\mu r_{s-1,t}\hat{a}_R + \nu r_{s,t+1}\hat{a}_I^\dagger) | st \rangle}{r_{km} + r_{st}} \\ - \langle km | (\mu\hat{a}_R^\dagger + \nu\hat{a}_I)(\mu\hat{a}_R + \nu\hat{a}_I^\dagger) | st \rangle \quad (87)$$

$$= \langle km | \left(\frac{2r_{s-1,t}}{r_{km} + r_{st}} - 1 \right) \mu^2 \hat{a}_R^\dagger \hat{a}_R | st \rangle \\ + \langle km | \left(\frac{2r_{s-1,t}}{r_{km} + r_{st}} - 1 \right) \nu \mu \hat{a}_I^\dagger \hat{a}_R^\dagger | st \rangle \\ + \langle km | \left(\frac{2r_{s,t+1}}{r_{km} + r_{st}} - 1 \right) \mu \nu \hat{a}_R \hat{a}_I | st \rangle \\ + \langle km | \left(\frac{2r_{s,t+1}}{r_{km} + r_{st}} - 1 \right) \nu^2 \hat{a}_I^\dagger \hat{a}_I | st \rangle \\ + \left(\frac{2\nu^2 r_{s+1,t}}{r_{km} + r_{st}} - \mu^2 \right) \langle km | st \rangle, \quad (88)$$

where μ and ν are defined in (48) and (49), respectively, (87) is derived using (62)-(67) in Appendix B, and (88) is due to the commutation relation $[\hat{a}, \hat{a}^\dagger] = 1$ and rearrangement of terms. Observe that the first, fourth, and fifth terms in (88) is not zero only when $\{k = s, m = t\}$, while the second and third terms are not zero when $\{k = s - 1, m = t - 1\}$ and $\{k = s + 1, m = t + 1\}$, respectively. Since

$$\frac{2r_{s-1,t}}{r_{km} + r_{st}} \Big|_{k=s, m=t} - 1 = \frac{1}{N_1} \quad (89)$$

$$\frac{2r_{s-1,t}}{r_{km} + r_{st}} \Big|_{k=s-1, m=t-1} - 1 = \frac{N_2 - N_1 - 1}{2N_1 N_2 + N_1 + N_2 + 1} \quad (90)$$

$$\frac{2r_{s,t+1}}{r_{km} + r_{st}} \Big|_{k=s+1, m=t+1} - 1 = \frac{N_2 - N_1 - 1}{2N_1 N_2 + N_1 + N_2 + 1} \quad (91)$$

$$\frac{2r_{s,t+1}}{r_{km} + r_{st}} \Big|_{k=s, m=t} - 1 = -\frac{1}{1 + N_2}, \quad (92)$$

we have:

$$\sum_{kmst} \frac{\langle \psi_{km} | \hat{\mathcal{L}}_R[\hat{a}^\dagger] \hat{\sigma}_{IR}(\eta) | \psi_{st} \rangle}{r_{km} + r_{st}} | \psi_{km} \rangle \langle \psi_{st} | = \hat{S}^\dagger(\zeta) \hat{K}_2 \hat{S}(\zeta), \quad (93)$$

where

$$\begin{aligned} \hat{K}_2 = & \left(\frac{N_2 - N_1 - 1}{2N_1 N_2 + N_1 + N_2 + 1} \right) \nu \mu \left(\hat{a}_I^\dagger \hat{a}_R^\dagger + \hat{a}_R \hat{a}_I \right) \\ & + \frac{\mu^2 \hat{a}_R^\dagger \hat{a}_R}{N_1} - \frac{\nu^2}{1 + N_2} \hat{a}_I^\dagger \hat{a}_I + \nu^2 \frac{N_2}{1 + N_2} - \mu^2. \end{aligned} \quad (94)$$

Combining (84) and (93) yields:

$$\hat{\Lambda}_\eta = \frac{1}{\eta} \hat{S}^\dagger(\zeta) \hat{K} \hat{S}(\zeta), \quad (95)$$

where

$$\hat{K} = (\bar{n}_B + 1) \hat{K}_1 + \bar{n}_B \hat{K}_2 \quad (96)$$

$$= C \hat{a}_R^\dagger \hat{a}_R + D \hat{a}_I^\dagger \hat{a}_I + E (\hat{a}_I^\dagger \hat{a}_R^\dagger + \hat{a}_R \hat{a}_I) + F, \quad (97)$$

and real constants

$$C = \mu^2 \frac{\bar{n}_B - N_1}{N_1(1 + N_1)} \quad (98)$$

$$D = \nu^2 \left(\frac{\bar{n}_B + 1 + N_2}{N_2(1 + N_2)} \right) \quad (99)$$

$$E = \mu \nu \left(\frac{N_1 - N_2 - 2\bar{n}_B - 1}{2N_1 N_2 + N_1 + N_2 + 1} \right) \quad (100)$$

$$F = \mu^2 \left(\frac{N_1 - \bar{n}_B}{1 + N_1} \right) - \nu^2 \left(\frac{\bar{n}_B + 1 + N_2}{1 + N_2} \right), \quad (101)$$

with μ , ν , N_1 , and N_2 defined in (48), (49), (55), and (56), respectively.

D. Eigenbasis of the SLD $\hat{\Lambda}_\eta$

Application of a two-mode squeezing operator $\hat{S}(\lambda e^{j\theta_\lambda})$ to a photon number operator $\hat{a}_I^\dagger \hat{a}_I$ results in:

$$\begin{aligned} & \hat{S}(\lambda e^{j\theta_\lambda}) \hat{a}_R^\dagger \hat{a}_R \hat{S}^\dagger(\lambda e^{j\theta_\lambda}) \\ &= \hat{S}(\lambda e^{j\theta_\lambda}) \hat{a}_R^\dagger \hat{S}^\dagger(\lambda e^{j\theta_\lambda}) \hat{S}(\lambda e^{j\theta_\lambda}) \hat{a}_R \hat{S}^\dagger(\lambda e^{j\theta_\lambda}) \\ &= (\kappa \hat{a}_R^\dagger + \xi e^{-j\theta_\lambda} \hat{a}_I)(\kappa \hat{a}_R + \xi e^{j\theta_\lambda} \hat{a}_I^\dagger) \\ &= \kappa^2 \hat{a}_R^\dagger \hat{a}_R + \kappa \xi (e^{j\theta_\lambda} \hat{a}_R \hat{a}_I + e^{-j\theta_\lambda} \hat{a}_I^\dagger \hat{a}_R^\dagger) + \xi^2 \hat{a}_I \hat{a}_I^\dagger, \end{aligned} \quad (102)$$

where $\kappa = \cosh \lambda$ and $\xi = \sinh \lambda$. Similarly,

$$\begin{aligned} & \hat{S}(\lambda e^{j\theta_\lambda}) \hat{a}_I^\dagger \hat{a}_I \hat{S}^\dagger(\lambda e^{j\theta_\lambda}) \\ &= \kappa^2 \hat{a}_I^\dagger \hat{a}_I + \kappa \xi (e^{-j\theta_\lambda} \hat{a}_I \hat{a}_R + e^{j\theta_\lambda} \hat{a}_I^\dagger \hat{a}_R^\dagger) + \xi^2 \hat{a}_R \hat{a}_R^\dagger. \end{aligned} \quad (103)$$

Thus, provided constants λ , F' , τ_1 , τ_2 exist, one can write:

$$\hat{K} = F' + \hat{S}(\lambda)(\tau_1 \hat{a}_R^\dagger \hat{a}_R + \tau_2 \hat{a}_I^\dagger \hat{a}_I) \hat{S}^\dagger(\lambda) \quad (104)$$

$$= F' + (\tau_1 \kappa \xi + \tau_2 \kappa \xi)(\hat{a}_R \hat{a}_I + \hat{a}_R^\dagger \hat{a}_I^\dagger) + \tau_1 \xi^2 + \tau_2 \xi^2 \quad (105)$$

$$+ (\tau_1 \kappa^2 + \tau_2 \xi^2) \hat{a}_R^\dagger \hat{a}_R + (\tau_1 \xi^2 + \tau_2 \kappa^2) \hat{a}_I^\dagger \hat{a}_I, \quad (106)$$

where (106) is from substituting (102) and (103) in (105) and rearranging terms. Note that it is necessary that $\theta_\lambda = 0$, which means that constants λ , F' , τ_1 , τ_2 must be real and satisfy:

$$C = \tau_1 \kappa^2 + \tau_2 \xi^2 \quad (107)$$

$$D = \tau_1 \xi^2 + \tau_2 \kappa^2 \quad (108)$$

$$E = (\tau_1 + \tau_2) \kappa \xi = (\tau_1 + \tau_2) \frac{\sinh 2\lambda}{2}, \quad (109)$$

$$F = F' + \tau_1 \xi^2 + \tau_2 \kappa^2 \quad (110)$$

where constants C , D , E , and F are given in (98)-(101). Now,

$$C - D = \tau_1(\kappa^2 - \xi^2) + \tau_2(\xi^2 - \kappa^2) = \tau_1 - \tau_2, \quad (111)$$

$$C + D = \tau_1(\kappa^2 + \xi^2) + \tau_2(\xi^2 + \kappa^2) = (\tau_1 + \tau_2) \cosh 2\lambda, \quad (112)$$

Furthermore,

$$\begin{aligned} (C + D)^2 - 4E^2 &= (\tau_1 + \tau_2)^2 (\cosh^2 2\lambda - \sinh^2 2\lambda) \\ &= (\tau_1 + \tau_2)^2. \end{aligned} \quad (113)$$

Using (111)-(113), one obtains:

$$\tau_1 = \frac{1}{2} (\sqrt{(C + D)^2 - 4E^2} + C - D) \quad (114)$$

$$\tau_2 = \frac{1}{2} (\sqrt{(C + D)^2 - 4E^2} - C + D) \quad (115)$$

$$\cosh 2\lambda = \frac{C + D}{\sqrt{(C + D)^2 - 4E^2}} \quad (116)$$

$$\sinh 2\lambda = \frac{2E}{\sqrt{(C + D)^2 - 4E^2}} \quad (117)$$

$$F' = F - (\tau_1 + \tau_2) \sinh^2(\lambda). \quad (118)$$

Finally, one can show that

$$\begin{aligned} & \hat{\Lambda}_\eta S^\dagger(\zeta) S(\lambda) | km \rangle \\ &= \frac{1}{\eta} S^\dagger(\zeta) \hat{K} S(\zeta) S^\dagger(\zeta) S(\lambda) | km \rangle \\ &= \frac{1}{\eta} S^\dagger(\zeta) [F' + S(\lambda)(\tau_1 \hat{a}_R^\dagger \hat{a}_R + \tau_2 \hat{a}_I^\dagger \hat{a}_I)^\dagger S(\lambda)^\dagger] S(\lambda) | km \rangle \\ &= \frac{1}{\eta} (F' + \tau_1 k + \tau_2 m) S^\dagger(\zeta) S(\lambda) | km \rangle, \end{aligned} \quad (119)$$

where

$$\lambda = \frac{1}{2} \log \left(\frac{2E + |C + D|}{\sqrt{(C + D)^2 - 4E^2}} \right). \quad (120)$$

Thus, $\hat{S}(\omega) | km \rangle$, $\omega = \lambda - \zeta$ is an eigenvector of the SLD $\hat{\Lambda}_\eta$.

REFERENCES

- [1] Z. Gong, C. N. Gagatsos, S. Guha, and B. A. Bash, "Fundamental limits of loss sensing over bosonic channels," in *Proc. IEEE Int. Symp. Inform. Theory (ISIT)*, virtual, Jul. 2021.
- [2] S. Pirandola, R. Laurenza, C. Ottaviani, and L. Banchi, "Fundamental limits of repeaterless quantum communications," *Nat. Commun.*, vol. 8, Apr. 2017.
- [3] R. Namiki, O. Gittsovich, S. Guha, and N. Lütkenhaus, "Gaussian-only regenerative stations cannot act as quantum repeaters," *Phys. Rev. A*, vol. 90, p. 062316, Dec. 2014.
- [4] B. M. Escher, R. L. de Matos Filho, and L. Davidovich, "General framework for estimating the ultimate precision limit in noisy quantum-enhanced metrology," *Nat. Phys.*, vol. 7, no. 5, pp. 406–411, May 2011.

[5] R. Demkowicz-Dobrzański, J. Kołodyński, and M. Guță, “The elusive Heisenberg limit in quantum-enhanced metrology,” *Nat. Commun.*, vol. 3, no. 1, p. 1063, Sep. 2012.

[6] S. M. Kay, *Fundamentals of Statistical Signal Processing, Volume I: Estimation Theory*, 1st ed. Upper Saddle River, NJ: Prentice Hall, 1993.

[7] A. K. Sinclair, E. Schroeder, D. Zhu, M. Colangelo, J. Glasby, P. D. Mauskopf, H. Mani, and K. K. Berggren, “Demonstration of microwave multiplexed readout of DC-biased superconducting nanowire detectors,” *IEEE Trans. Appl. Supercond.*, vol. 29, no. 5, Aug. 2019.

[8] A. N. McCaughan, D. M. Oh, and S. W. Nam, “A stochastic SPICE model for superconducting nanowire single photon detectors and other nanowire devices,” *IEEE Trans. Appl. Supercond.*, vol. 29, no. 5, Aug. 2019.

[9] J. Lee, L. Shen, A. Cerè, T. Gerrits, A. E. Lita, S. W. Nam, and C. Kurtsiefer, “Multi-pulse fitting of transition edge sensor signals from a near-infrared continuous-wave source,” *Rev. Sci. Instrum.*, vol. 89, no. 12, p. 123108, 2018.

[10] M. A. Nielsen and I. L. Chuang, *Quantum Computation and Quantum Information*. New York, NY, USA: Cambridge University Press, 2000.

[11] M. Wilde, *Quantum Information Theory*, 2nd ed. Cambridge University Press, 2016, arXiv:1106.1445v7.

[12] M. O. Scully and M. S. Zubairy, *Quantum Optics*. Cambridge, UK: Cambridge University Press, 1997.

[13] G. S. Agarwal, *Quantum Optics*. Cambridge, UK: Cambridge University Press, 2012.

[14] M. Orszag, *Quantum Optics*, 3rd ed. Berlin, Germany: Springer, 2016.

[15] C. L. Degen, F. Reinhard, and P. Cappellaro, “Quantum sensing,” *Rev. Mod. Phys.*, vol. 89, p. 035002, Jul 2017.

[16] S. Pirandola, B. R. Bardhan, T. Gehring, C. Weedbrook, and S. Lloyd, “Advances in photonic quantum sensing,” *Nat. Photon.*, vol. 12, no. 12, pp. 724–733, Dec. 2018.

[17] A. Monras and M. G. A. Paris, “Optimal quantum estimation of loss in bosonic channels,” *Phys. Rev. Lett.*, vol. 98, p. 160401, Apr. 2007.

[18] G. Adesso, F. Dell’Anno, S. De Siena, F. Illuminati, and L. A. M. Souza, “Optimal estimation of losses at the ultimate quantum limit with non-gaussian states,” *Phys. Rev. A*, vol. 79, p. 040305, Apr 2009.

[19] C. Weedbrook, S. Pirandola, R. García-Patrón, N. J. Cerf, T. C. Ralph, J. H. Shapiro, and S. Lloyd, “Gaussian quantum information,” *Rev. Mod. Phys.*, vol. 84, pp. 621–669, May 2012.

[20] A. Monras and F. Illuminati, “Measurement of damping and temperature: Precision bounds in gaussian dissipative channels,” *Phys. Rev. A*, vol. 83, p. 012315, Jan. 2011. [Online]. Available: <https://link.aps.org/doi/10.1103/PhysRevA.83.012315>

[21] R. Nair and M. Gu, “Fundamental limits of quantum illumination,” *Optica*, vol. 7, no. 7, pp. 771–774, Jul. 2020.

[22] S. Lloyd, “Enhanced sensitivity of photodetection via quantum illumination,” *Science*, vol. 321, no. 5895, pp. 1463–1465, 2008.

[23] S.-H. Tan, B. I. Erkmen, V. Giovannetti, S. Guha, S. Lloyd, L. Maccone, S. Pirandola, and J. H. Shapiro, “Quantum illumination with gaussian states,” *Phys. Rev. Lett.*, vol. 101, p. 253601, Dec. 2008.

[24] S. Guha and B. I. Erkmen, “Gaussian-state quantum-illumination receivers for target detection,” *Phys. Rev. A*, vol. 80, p. 052310, Nov. 2009.

[25] J. H. Shapiro, “The quantum illumination story,” *IEEE Aerosp. Electron. Syst. Mag.*, vol. 35, no. 4, pp. 8–20, 2020.

[26] M. Sanz, U. Las Heras, J. J. García-Ripoll, E. Solano, and R. Di Candia, “Quantum estimation methods for quantum illumination,” *Phys. Rev. Lett.*, vol. 118, p. 070803, Feb. 2017.

[27] R. Jonsson and R. D. Candia, “Gaussian quantum estimation of the lossy parameter in a thermal environment,” arXiv:2203.00052 [quant-ph], 2022.

[28] B. A. Bash, D. Goeckel, and D. Towsley, “Square root law for communication with low probability of detection on AWGN channels,” in *Proc. IEEE Int. Symp. Inform. Theory (ISIT)*, Cambridge, MA, Jul. 2012.

[29] —, “Limits of reliable communication with low probability of detection on AWGN channels,” *IEEE J. Sel. Areas Commun.*, vol. 31, no. 9, pp. 1921–1930, 2013.

[30] B. A. Bash, D. Goeckel, S. Guha, and D. Towsley, “Hiding information in noise: Fundamental limits of covert wireless communication,” *IEEE Commun. Mag.*, vol. 53, no. 12, 2015.

[31] B. A. Bash, A. H. Gheorghe, M. Patel, J. L. Habif, D. Goeckel, D. Towsley, and S. Guha, “Quantum-secure covert communication on bosonic channels,” *Nat. Commun.*, vol. 6, Oct. 2015.

[32] B. A. Bash, C. N. Gagatsos, A. Datta, and S. Guha, “Fundamental limits of quantum-secure covert optical sensing,” in *Proc. IEEE Int. Symp. Inform. Theory (ISIT)*, Aachen, Germany, Jun. 2017.

[33] C. N. Gagatsos, B. A. Bash, A. Datta, Z. Zhang, and S. Guha, “Covert sensing using floodlight illumination,” *Phys. Rev. A*, vol. 99, p. 062321, Jun. 2019.

[34] M. S. Bullock, C. N. Gagatsos, S. Guha, and B. A. Bash, “Fundamental limits of quantum-secure covert communication over bosonic channels,” *IEEE J. Sel. Areas Commun.*, vol. 38, no. 3, pp. 471–482, Mar. 2020.

[35] C. N. Gagatsos, M. S. Bullock, and B. A. Bash, “Covert capacity of bosonic channels,” *IEEE J. Sel. Areas Inf. Theory*, vol. 1, pp. 555–567, Aug. 2020.

[36] R. D. Gill and S. Massar, “State estimation for large ensembles,” *Phys. Rev. A*, vol. 61, p. 042312, Mar. 2000.

[37] M. Hayashi and K. Matsumoto, “Statistical model with measurement degree of freedom and quantum physics,” in *Asymptotic Theory of Quantum Statistical Inference: Selected Papers*, M. Hayashi, Ed. Singapore: World Scientific Publishing Co. Pte. Ltd., 2005, pp. 162–169.

[38] M. Hayashi, *Quantum Information Theory: Mathematical Foundation*. Springer-Verlag Berlin Heidelberg, 2017.

[39] S. Pirandola, “Quantum reading of a classical digital memory,” *Phys. Rev. Lett.*, vol. 106, p. 090504, Mar. 2011.

[40] J. H. Shapiro, S. Guha, and B. I. Erkmen, “Ultimate channel capacity of free-space optical communications,” *IEEE J. Opt. Netw.*, vol. 4, no. 8, pp. 501–516, Aug. 2005.

[41] P. Marian and T. A. Marian, “Uhlmann fidelity between two-mode gaussian states,” *Phys. Rev. A*, vol. 86, p. 022340, Aug. 2012.

[42] L. Banchi, S. L. Braunstein, and S. Pirandola, “Quantum fidelity for arbitrary gaussian states,” *Phys. Rev. Lett.*, vol. 115, p. 260501, Dec. 2015.

[43] C. W. Helstrom, *Quantum Detection and Estimation Theory*. New York, NY, USA: Academic Press, Inc., 1976.

[44] Z. Jiang, “Quantum fisher information for states in exponential form,” *Phys. Rev. A*, vol. 89, p. 032128, Mar. 2014.

[45] T. Eberle, V. Händchen, and R. Schnabel, “Stable control of 10 db two-mode squeezed vacuum states of light,” *Opt. Express*, vol. 21, no. 9, pp. 11 546–11 553, May 2013.

[46] A. J. Miller, S. W. Nam, J. M. Martinis, and A. V. Sergienko, “Demonstration of a low-noise near-infrared photon counter with multiphoton discrimination,” *Appl. Phys. Lett.*, vol. 83, no. 4, pp. 791–793, 2003.

[47] Z. Zhang, S. Mouradian, F. N. C. Wong, and J. H. Shapiro, “Entanglement-enhanced sensing in a lossy and noisy environment,” *Phys. Rev. Lett.*, vol. 114, p. 110506, Mar. 2015. [Online]. Available: <https://link.aps.org/doi/10.1103/PhysRevLett.114.110506>

[48] S. Guha, “Classical capacity of the free-space quantum-optical channel,” Master’s thesis, Massachusetts Institute of Technology, 2004.

[49] I. Gradshteyn and I. Ryzhik, *Table of Integrals, Series, and Products*, 7th ed., A. Jeffrey and D. Zwillinger, Eds. Elsevier Academic Press, 2007.

[50] M. D. Eisaman, J. Fan, A. Migdall, and S. V. Polyakov, “Invited review article: Single-photon sources and detectors,” *Rev. Sci. Instrum.*, vol. 82, no. 7, p. 071101, 2011.

[51] U. Sinha, S. N. Sahoo, A. Singh, K. Joarder, R. Chatterjee, and S. Chakraborti, “Single-photon sources,” *Opt. Photon. News*, vol. 30, no. 9, pp. 32–39, Sep. 2019.

[52] E. Meyer-Scott, C. Silberhorn, and A. Migdall, “Single-photon sources: Approaching the ideal through multiplexing,” *Rev. Sci. Instrum.*, vol. 91, no. 4, p. 041101, 2020.

[53] J. W. Pearson, S. Olver, and M. A. Porter, “Numerical methods for the computation of the confluent and gauss hypergeometric functions,” *Numer. Algorithms*, vol. 74, no. 3, pp. 821–866, Mar. 2017.

[54] H. L. Van Trees, *Detection, Estimation, and Modulation Theory, Part I: Detection, Estimation, and Linear Modulation Theory*. New York: John Wiley & Sons, Inc., 2001.

[55] F. Hong-yi and F. Yue, “Representations of two-mode squeezing transformations,” *Phys. Rev. A*, vol. 54, pp. 958–960, Jul. 1996.

[56] A. Ferraro, S. Olivares, and M. G. A. Paris, *Gaussian States in Quantum Information*, ser. Napoli Series on physics and Astrophysics. Napoli, Italy: Bibliopolis, 2005, <https://arxiv.org/abs/quant-ph/0503237>.